ELSEVIER

Contents lists available at ScienceDirect

Intermetallics

journal homepage: http://www.elsevier.com/locate/intermet





A new thermodynamic modeling of the Ti–V system including the metastable $\boldsymbol{\omega}$ phase

Biao Hu^{a,b}, Soumya Sridar^b, Liangyan Hao^b, Wei Xiong^{b,*}

- ^a School of Materials Science and Engineering, Anhui University of Science and Technology, Huainan, Anhui, 232001, PR China
- b Physical Metallurgy and Materials Design Laboratory, Department of Mechanical Engineering and Materials Science, University of Pittsburgh, Pittsburgh, PA, 15261, IISA

ARTICLE INFO

Keywords: Ti–V ω phase Lattice stability CALPHAD Ti alloys Martensitic transformation

ABSTRACT

A new thermodynamic model based on the Einstein function with more physical significance is used to describe the hcp, bcc, fcc, ω , liquid and amorphous phases for Ti and V from above the melting point down to 0 K by the CALPHAD (CALculation of PHAse Diagrams) approach for the third generation thermodynamic databases. The liquid and amorphous phases are treated as one phase using the generalized two-state model. The Debye temperatures and the enthalpy differences at 0 K for different allotropes of Ti and V have been computed by *ab initio* calculations. The Ti–V system has been reassessed based on the new Gibbs energy functions for Ti and V obtained in the present work and experimental data available in the literature. The martensitic transformation and metastable ω phase formation in the Ti–V system at low temperature are thermodynamically described. The new description can better represent both the phase equilibria data and the temperatures of martensitic transformation and ω formation. The metastable phase diagram of the Ti–V system as well as the $T_0(\beta/\omega)$ curves have been calculated using the obtained thermodynamic parameters. The calculated results indicate that most of the reliable experimental data are satisfactorily reproduced in the present modeling.

1. Introduction

The Gibbs free energy functions for pure elements from the SGTE database compiled by Dinsdale [1] have been widely adopted in the CALPHAD community till now. In the first and second generations of thermodynamic databases, the Gibbs energy for each phase is described as a simple function of temperature, pressure and composition. Although the temperature range for the Gibbs energy functions are from room temperature to 6000 K, the description is mainly applied in intermediate temperature range and hardly reliable below 600 K or above the melting point. This makes it impossible to achieve a reliable description for phase transformation at lower temperature, such as martensitic transformation and ω phase transition in Ti alloys. A new thermodynamic model with definite physical meaning will improve the possibility to describe these low temperature phase transformations. Therefore, the third generation CALPHAD databases based on the Einstein model have been developed in order to achieve the reliable thermodynamic description from 0 K up to temperatures above the melting point. The first attempt to define this new thermodynamic model was at Ringberg workshop in 1995 [2-5]. Subsequently, this model was improved by

Chen and Sundman [6] to describe thermodynamic properties for bcc, fcc, liquid and amorphous phases of pure Fe. Recently, this new model [6] has been successfully applied to other unaries, such as Mn [7], metastable hcp phase of Fe and Mn [8], Co [9,10], Pb [11], C [12], Al [13,14], Sn [15], Au [16], Zn [17], Cr and Ni [18]. The advantages of the third generation lattice stability has also been demonstrated in some critical binary systems such as Fe–Cr and Cr–Ni [18–20].

Due to the attractive properties such as high specific strength, good corrosion resistance and excellent toughness, Ti alloys have been extensively utilized in aviation, aerospace, automotive and chemical industries [21–24]. With increasing content of β stabilizing elements like V, Mo, Nb, two kinds of martensite, i.e. the hexagonal close packed (hcp) α' (P6 $_3$ /mmc) and the orthorhombically-distorted α'' (Cmcm), have been identified in Ti alloys that were rapidly quenched from the body-centered cubic (bcc) β phase. The α' martensitic phase usually forms at lower concentrations of β stabilizing elements while the α'' martensitic phase occurs at higher concentrations. The major difference between the $\beta \to \alpha''$ and $\beta \to \alpha'$ transformations is that the degree of displacement in atomic shuffle during the former transformation is less than the latter. Therefore, the $\beta \to \alpha''$ transformation can be considered

E-mail addresses: weixiong@pitt.edu, w-xiong@outlook.com (W. Xiong).

^{*} Corresponding author.

Table 1
Summary of the heat capacity of titanium.

Temperature interval, K	Phase	Method	Purity of Ti, wt.%	Reference
51–298	hcp Calorimetry		98.75	Kelley [36]
15-305	hcp	Drop calorimetry	99.96	Kothen and Johnston [37]
4–15	hcp	Adiabatic calorimetry	99.95	Aven et al. [38]
1.2-20	hcp	Calorimetry	99.90	Wolcott [39]
20-200	hcp	Vacuum calorimetry	99.00	Burk et al. [40]
12-273	hcp	Adiabatic calorimetry	99.90	Clusius and Franzosini [41]
1.1-4.5	hcp	Adiabatic calorimetry	99.86	Kneip et al. [42]
1.2-4.5	hcp	Calorimetry	99.92	Hake and Cape [43]
1.5-5.3	hcp	Calorimetry	99.86	Collings and Ho [44]
1.2-4.5	hcp	Adiabatic calorimetry	99.80	Agarwal and Betterton [45]
400-1100	hcp	Drop calorimetry	n/a	Golutvin [47]
280-1150	hcp	Drop calorimetry	n/a	Serebrennikov and Gel'd [48]
187-353	hcp	Adiabatic calorimetry	n/a	Stalinski and Bieganski [49]
340-1100	hcp	Electrical resistivity technique	99.99	Parker [50]
297-1075	hcp	Adiabatic calorimetry	99.95	Novikov [51]
293-473	hcp	Calorimetry	99.90	Zarichnyak and Lisnenko [52]
320-1020	hcp	Adiabatic calorimetry	99.94	Cash and Brooks [53]
600-1066	hcp	Modulation calorimetry	n/a	Holland [54]
873-1873	hcp, bcc	Adiabatic vacuum calorimetry	99.00	Backhurst [55]
300-1900	hcp, bcc	Calorimetry	n/a	Maglic and Pavicic [56]
320-1800	hcp, bcc	Adiabatic calorimetry	99.80	Kohlhaas et al. [57]
920-1370	hcp, bcc	Longitudinal thermal flux method	n/a	Peletskii and Zaretskii [58]
300-1300	hcp, bcc	Differential scanning calorimeter	n/a	Takahashi [59]
1400-1880	bcc	Modulation calorimetry	n/a	Shestopal [60]
1000-1700	bcc	Thermal relaxation calorimeter	99.80	Arutyunov et al. [61]
1500-1900	bcc	Pulse heating calorimetry	99.60	Kaschnitz and Reiter [62]
1500-1900	bcc	Pulse heating calorimetry	99.90	Cezairliyan and Miiller [63]
1300-1800	bcc	Modulated power method	99.99	Guo et al. [64]
1969-2315	liquid	Levitation calorimetry	99.95	Treverton and Margrave [67]
1940-2045	liquid	Drop calorimetry	99.91	Berezin et al. [68]
1650-2000	liquid	Electrostatic levitator	99.99	Paradis and Rhim [69]
1650-1950	liquid	Electrostatic levitator	99.995	Lee et al. [70]
1815-2211	liquid	Drop calorimetry	99.999	Zhou et al. [71]
1943	liquid	Electrostatic levitator	99.90	Ishikawa et al. [72]
250-2100	hcp, bcc	Assessment	n/a	Hultgren et al. [65]
400-2300	hcp, bcc, liquid	Assessment	n/a	Glushko et al. [66]
0-3600	hcp, bcc, liquid	Assessment	n/a	NIST-JANAF [46]
1-3800	hcp, bcc, liquid	Assessment	n/a	Desai [35]
50-1500	fcc	DFT	100	Zhang et al. [73]
0-1200	ω	DFT	100	Mei et al. [74]
0-1200	ω	DFT	100	Argaman et al. [75]

as a crystallographically incomplete $\beta \to \alpha'$ transformation. In pure titanium, the metastable phase ω with hexagonal structure forms only under large compressive stress. In contrast, the ω phase forms as a transition phase only at ambient pressure in alloys containing sufficient concentrations of β stabilizing elements when they are quenched from high temperature β solid solution which is known as athermal ω or aged at a low temperature that is known as isothermal ω . The ω phase has been observed in Ti alloys in a composition very close to martensitic transformations. The ω phase precipitation is competitive to martensitic transformation [25]. In recent years, ω formation has gained wide attention due to its role as a precursor to fine scale α phase precipitation in Ti-alloys [26–31]. V is one of the most common β isomorphous alloying elements in Ti alloys, exerting a beneficial effect on their plasticity and strength [32]. The thermodynamic description of the martensitic transformation and ω phase precipitation in the Ti–V alloys based on the third generation thermodynamic parameters for titanium and vanadium is fundamental to the design of new Ti-V based alloys. In the present work, the thermodynamic model from Chen and Sundman [6] is accepted to describe the hcp, bcc, fcc, ω, liquid and amorphous phases of Ti and V, and further the Ti-V system is reassessed. This modeling effort will be beneficial in calculating the martensitic transformation and ω phase transition in the Ti–V alloys.

Therefore, the purposes of the present work are (1) to critically evaluate the literature data for pure elements Ti, V and the Ti–V binary system, (2) to compute the Debye temperatures and the enthalpy

differences at 0 K for different allotropes of Ti and V by *ab initio* calculations to supply the necessary thermodynamic data for the modeling, (3) to develop the third generation thermodynamic parameters for pure Ti and V using a new model with more physical significance from high temperature down to 0 K, and (4) to reassess the Ti–V binary system and calculate its metastable phase diagram as well as the $T_0(\beta/\alpha)$ and $T_0(\beta/\alpha)$ curves by means of the CALPHAD approach [33,34].

2. Literature review

2.1. Pure titanium

Titanium has two stable allotropes, i.e. the low-temperature phase $\alpha\textsc{-Ti}$ with hcp structure isotypic with Mg and the high-temperature phase $\beta\textsc{-Ti}$ with bcc structure isotypic with W. The widely accepted transition temperature between hcp and bcc is 1155 K [1]. The melting point of titanium is 1941 K and the atomic weight is 47.88 [1].

The thermodynamic properties including heat capacity, enthalpies of formation, transformation and fusion, entropy, etc., of pure titanium have been critically reviewed and discussed by Desai [35] based on the experimental data available in the literature. Desai [35] recommended the values of heat capacity covering the temperature range from 1 to 3800 K and the values of enthalpy, entropy as well as the Gibbs energy covering the temperature range from 298.15 to 3800 K. The thermodynamic properties of titanium collected from literature are summarized

 Table 2

 Debye temperature, Einstein temperature and electronic specific heat coefficient for different allotropes of titanium.

Phase	$\theta_{\rm D}(-3),~{\rm K}$	$\theta_{\rm D}(0),{\rm K}^{\rm a}$	θ E, K ^b	γ, mJ/mol⋅K	Reference
hcp	423	376.47	268.80	3.11	Agarwal and Betterton [79]
	428 ± 5	380.92	271.98	3.32 ± 0.02	Agarwal and Betterton [45]
	427	380.03	271.34	3.346	Kneip et al. [42]
	421	374.69	267.53	3.38	Aven et al. [38]
	429 ± 7	381.81	272.61	3.305	Hake and Cape [43]
	415	369.35	263.72	3.30	Heiniger and Muller [80]
	430	382.7	273.25	3.56	Wolcott [39]
	410	364.90	260.54	3.32	Collings and Ho [44]
	420	373.80	266.89	3.36	Collings and Ho [81]
	412 ± 5	366.68	261.81	3.31 ± 0.03	Dummer [82]
	428 ± 5	380.92	271.98	3.349	Fisher and Renken [83]
	425 ± 5	378.25	270.07	3.332 ± 0.02	Desai [35]
	420	373.80	266.89	3.35	Kittel [84]
	403	358.67	256.09		Argaman et al. [75]
		374	267.04		Chen and Sundman [85]
		385	274.89		Chen and Sundman [78]
	397	53.33	252.28		This work (DFT)
			269.66	7.77 ^c	This work (CALPHAD)
bcc		272	194.21		Petry et al. [86]
		264.2	188.64		Ledbetter et al. [87]
		281.3	200.85		Zhang et al. [73]
		263	187.78		Chen and Sundman [85]
		269	192.07		Chen and Sundman [78]
			192.01	3.51 ^c	This work (CALPHAD)
fcc		312	222.77		Chen and Sundman [78]
	371	330.19	235.76		This work (DFT)
			236.67	2.20°	This work (CALPHAD)
ω	457	406.73	290.41		Argaman et al. [75]
			287.50		Yan and Olson [88]
	439	390.71	278.97		Hu et al. [89]
	475	422.75	301.84		This work (DFT)
			289.3	3.51 ^c	This work (CALPHAD)
liquid-amorphous	300	267.00	190.64		Ristić et al. [93,94], Bakonyi [95]
-	330 ± 30^{c}	294 ± 27	210 ± 19		Grimvall [96]
			185.76	4.01°	This work (CALPHAD)

 $[^]a\theta_D(0)$ is derived from 0.89· $\theta_D(-3)$ [78] when $\theta_D(0)$ is not available in the literature.

as follows.

The reported heat capacities of titanium are summarized in Table 1. The low temperature heat capacities of titanium between 0 and 300 K were measured by many groups of researchers [36-45] using different calorimetric techniques. Their experimental results show very good agreement with each other in the temperature interval between 0 and 300 K. The recommended values of heat capacity between 0 and 300 K from the work of NIST-JANAF edited by Chase [46] and Desai [35] agree well with the measurements [36–45] with the deviation of $\pm 1.5\%$. The high temperature heat capacities for hcp titanium in the temperature range from 300 to 1155 K have been experimentally investigated in numerous works [47-59]. By comparing the experimental data as a whole, there is a general consistency among the different works [49, 51–53,57]. The experimental results from Golutvin [47], Serebrennikov and Gel'd [48], Parker [50] and Holland [54] are scattered and higher than the values from the works [49,51-53,57], which are not accepted to optimize thermodynamic parameters in the present work. Although Backhurst [55], Takahashi [59] and Peletskii and Zaretskii [58] reported some similar results, their values are much higher at the transition temperature between hcp and bcc and lower at other temperatures, which are also not accepted in the present work. The experimental investigations of the high temperature heat capacity for bcc titanium in the temperature range from 1155 K to the melting point have been reported by several works [55-64]. These experimental data are scattered in the whole temperature range. As mentioned above, the experimental results from Backhurst [55] and Peletskii and Zaretskii [58] are lower than the other works [57,62,64]. The data from Shestopal [60] and

Maglic and Pavicic [56] were unusual and increase quickly when the temperature is above 1800 K. Thus, the experimental data from the works [55,56,58,60] are not included in the present work. Based on the experimental heat capacity of hcp and bcc available in the literature, Hultgren et al. [65], Glushko et al. [66], NIST-JANAF [46] and Desai [35] recommended the values of heat capacity of hcp and bcc titanium, which are consistent with each other. In addition, Desai [35] discussed the deviation between experimental heat capacity [50–55,57,58,60,61,63] and recommended values. The heat capacities recommended by Desai [35] are accepted in the present work since these values can reproduce well with most of the reliable experimental data.

The experimental and recommended heat capacities of liquid titanium were reported in different works [35,46,66–72] with different constant values. The value reported by Zhou et al. [71] is 33.64 J/(mol·K), which is much lower than the one from other works. Glushko et al. [66], NIST-JANAF [46] and Desai [35] recommended the values of heat capacity for liquid titanium to be 48.80, 47.237 and 46.29 J/(mol·K), respectively. Since the experimental heat capacity are scattered and the recommended values from Desai [35] are between the experimental data from Treverton and Margrave [67], Berezin et al. [68], Paradis and Rhim [69], and Ishikawa et al. [72], the recommended value of heat capacity for liquid titanium from Desai [35] is adopted in the present optimization of the parameters for the liquid phase.

No experimental heat capacities for the metastable fcc and ω titanium are available in the literature. The temperature dependence of the heat capacities for fcc titanium at different pressures were studied by Zhang et al. [73] using the first-principles plane-wave pseudopotential

 $^{{}^{\}rm b}\theta_{\rm E}$ is derived from 0.714· $\theta_{\rm D}(0)$ [76].

^cThe optimized value for a in Eq. (4), which consists of electronic excitations and low-order anharmonic vibrational contributions (dilatational and explicitly anharmonic).

 $^{^{}d}\theta_{D}(-3)$ of amorphous state is lower by 15–30% of the one of crystalline state, which was assumed by Grimvall [96].

Table 3Summary of the enthalpy and entropy of titanium.

$\Delta H_{ ext{hcp-bcc}}$, J/mol	$\Delta_{\rm fus}H^{\rm o}$, J/mol	H°(298.15 K)–H°(0 K), J/mol	S ^o (298.15 K), J/ (mol·K)	$\Delta S_{\text{hcp-bcc}}$, J/ (mol·K)	$\Delta_{\rm fus}S^{\rm o},~{ m J/} \ ({ m mol\cdot K})$	Method	Reference
4170 ± 200				3.58		Pulse heating calorimetry	Cezairliyan and Miller
4255						Assessment	Hultgren et al. [65]
4090 ± 100						Adiabatic calorimetry	Scott [102]
3350 ± 200						Pulse heating calorimetry	Parker [50]
3430 ± 80						Drop calorimetry	Golutvin [47]
4150						Adiabatic calorimetery	Kohlhaas et al. [57]
3946		4813	30.699			Drop calorimetry	Kothen [103]
3800						Assessment	Glushko et al. [66]
4175						Droxp calorimetry	Gel'd and Putintsev [104]
4213						DTA	Harmelin and Lehr [105]
4360 ± 100						longitudinal thermal flux	Peletskii and Zaretskii
						method	[58]
3680						Adiabatic vacuum calorimetry	Backhurst [55]
4303						Pulse heating calorimetry	Kaschnitz and Reiter
4300	18000					Pulse heating calorimetry	Martynyuk and Tsapkov
	$14146 \pm \\480$					Drop calorimetry	Berezin et al. [68]
	13226 ± 500				6.823 ± 0.25	Levitation calorimetry	Treverton and Margrave [67]
	14980					Levitation calorimetry	Bonnel [108]
	14300					Electrostatic levitator	Paradis and Rhim [69]
4170 ± 200	14550 ± 500	4822 ± 10	30.686 ± 0.08	3.576 ± 0.172	7.481 ± 0.25	Assessment	Desai [35]
4172	14146	4830	30.759 ± 0.20	3.578	7.295	Assessment	NIST-JANAF [46]
4170	14146	4824	30.72	3.6104	7.288	CALPHAD	SGTE [1]
4175	14277	4824	30.6	3.615	7.355	CALPHAD	This work

method combined with the quasi-harmonic Debye model based on density functional theory (DFT). The calculated results show that the heat capacity rapidly increases at low temperatures (below 400 K), whereas when the pressure increases from 0 to 80 GPa, the heat capacity decreases. The heat capacity for the ω phase at constant pressure was calculated by Mei et al. [74] and Argaman et al. [75] within the DFT using phonon density of state (DOS) and Debye model. The calculated results from Mei et al. [74] and Argaman et al. [75] are very consistent with each other. The heat capacities for the fcc and ω titanium estimated using theoretical calculations from the works [73–75] are accepted in the present work.

Einstein temperature θ_E for different phases of titanium is the key parameter for the third generation thermodynamic database. However, the Einstein temperature cannot be determined directly from experiments. According to the empirical formula, Einstein temperature is about 0.714 times the high temperature entropy Debye temperature $\theta_D(0)$ [6,76], i.e., $\theta_E \approx 0.714\theta_D(0)$. $\theta_D(0)$ is a special case of the Debye temperatures $\theta_D(n)$ derived from the nth moment of the phonon frequencies [77]. For an ideal Debye solid, all $\theta_D(n)$ values are equal to the low temperature limit of the Debye temperature $\theta_{\rm D}(-3)$ that can be obtained from low-temperature heat capacity or elastic constants. For a real solid, $\theta_D(0)$ is different from $\theta_D(-3)$ and the ratio $\theta_D(0)/\theta_D(-3)$ appears to be constant for the same element [6]. The value of $\theta_{\rm D}(0)/\theta_{\rm D}(-3)$ ratio was reported to be 0.89 for hcp titanium by Chen and Sundman [78] and it is assumed to be the same for hcp, bcc, fcc, ω and liquid-amorphous titanium in the present work. The low temperature limit of the Debye temperature $\theta_D(-3)$, the high temperature entropy Debye temperature $\theta_D(0)$, Einstein temperature θ_E and electronic specific heat coefficient γ for different phases of titanium are summarized in Table 2. The low temperature limit of the Debye temperature $\theta_D(-3)$ of the hcp titanium has been reported by many researchers [35,38,39, 42–45,75,78–85]. Their results are in good agreement with each other. The high temperature entropy Debye temperature $\theta_D(0)$ and Einstein temperature θ_E are derived from the relations $\theta_D(0) = 0.89\theta_D(-3)$ [78]

and $\theta_{\rm E}=0.714\theta_{\rm D}(0)$ [76], respectively. For the bcc phase, the Debye temperatures $\theta_D(0)$ were reported by Petry et al. [86], Ledbetter et al. [87], Zhang et al. [73] and Chen and Sundman [78,85]. As can been seen from Table 2, the reported Debye temperature $\theta_D(0)$ values for bcc titanium are consistent with each other. For the metastable fcc and $\boldsymbol{\omega}$ titanium, their Debye temperatures $\theta_D(-3)$ or $\theta_D(0)$ were estimated using DFT [75,78,88,89]. The Debye temperature of the liquid-amorphous phase for titanium is not available in the literature. In this work, two approaches are recommended to estimate the Debye temperature of the liquid-amorphous phase for pure element. In the first method, the Debye temperature of the liquid-amorphous phase for pure element can be extrapolated by linear fitting of the Debye temperatures of related binary amorphous alloys. The Debye temperatures of amorphous Ni-Ti [90,91] and Cu-Ti [92] alloys were measured. The Debye temperature with respect to compositions for Ni and Cu in the Ni-Ti and Cu-Ti systems, respectively, can be utilized for the fitting procedure [93-95]. Thus, the Debye temperature of the amorphous phase for pure titanium can be obtained. The second method is the assumption from Grimvall [96] that the Debye temperature θ_D (-3) of amorphous state is lower by 15-30% of the one of crystalline state, which was established based on the experiments [97-99] and theory [100]. The Debye temperature of amorphous titanium according to this assumption was found to be 300 K, which is consistent with the value 330 \pm 30 K extrapolated from the Debve temperatures of amorphous Ni-Ti and Cu-Ti allovs.

The enthalpies and entropies of transition and fusion for titanium are summarized in Table 3. The enthalpy of transition between the hcp and bcc phases $\Delta H_{\text{hcp-bcc}}$ has been reported in numerous works [47,50,55,57,58,65,66,101–107]. Hultgren et al. [65], Desai [35] and Chase [46] recommended the values of $\Delta H_{\text{hcp-bcc}}$ to be 4255, 4170 \pm 200 and 4172 J/mol, respectively, based on the pulse heating measurements from Cezairliyan and Miller [101]. The recommended values of $\Delta H_{\text{hcp-bcc}}$ agree well with the experimental data from Scott [102], Kohlhaas et al. [57], Gel'd and Putintsev [104], Harmelin and Lehr [105], Peletskii and Zaretskii [58], Kaschnitz and Reiter [106] and Martynyuk and Tsapkov

Table 4 The ground state energy differences for bcc, fcc and ω relative to hcp titanium at 0 K from DFT calculations and CALPHAD approach.

_	$\Delta E_{ m bcc-hcp}$, J/mol	$\Delta E_{ m fcc-hcp}, \ { m J/mol}$	$\Delta E_{\omega ext{-hcp}},$ J/mol	Method	Reference
	10556 10295	5509	-203	QHA ^a and Debye model PAW-GGA ^b	Mei et al. [74] Wang et al. [109]
	10517 7062	6770	-579	QHA Extrapolation based on Einstein model	Hu et al. [89] Vřešťál et al. [110]
			-788	BP-GGA ^c	Argaman et al. [75]
	9649	5403 6000	-1351	DFT CALPHAD	OQMD [111] SGTE [1]
	10619	5438	-571	DFT	This work
	6029	5910	-214	CALPHAD	This work

^a QHA: Quasiharmonic Approximation.

[107]. The enthalpy of fusion $\Delta_{fus}H^0$ for titanium was experimentally investigated by several groups [67-69,107,108]. NIST-JANAF [46] recommended the value of $\Delta_{fus}H^{o}$ to be 14146 J/mol based on the drop calorimetry measurements by Berezin et al. [68], while Desai [35] recommended it to be 14550 \pm 500 J/mol by extrapolating solid and liquid enthalpies to the melting point. It is found that both the values were consistent with each other. Desai [35] deduced the value for H^o(298.15 K)– $H^0(0~{\rm K})$ to be 4822 $\pm~10~{\rm J/mol}$ according to the recommended heat capacity C_D values and also deduced the value for $S^0(298.15 \text{ K})$ to be 30.686 \pm 0.08 J/(mol K) by integration of C_p /T values, which are in agreement with the values 4830 J/mol and 30.759 \pm 0.20 J/(mol·K), respectively, recommended from NIST-JANAF [46]. For the entropies of transition $\Delta S_{hcp-bcc}$ and fusion $\Delta_{fus}S^{0}$, Desai [35] and NIST-JANAF [46] also recommended their values 3.576 \pm 0.172 and 7.481 \pm 0.25 J/(mol·K), and 3.578 and 7.295 J/(mol·K), respectively, by integration of C_p/T and $S^0(298.15 \text{ K})$. In addition, $H_m(T) - H_m(298.15 \text{ K})$ and $S_m(T) - S_m(298.15 \, K)$ values for titanium were investigated by several groups [67,68,106] and their experimental results are consistent with each other. The recommended values for heat capacity, enthalpies and entropies of transition and fusion by Desai [35] are accepted in the present work since they are self-consistent and in good agreement with the most of reported experimental data.

There is no experimental information for the Gibbs energies of bcc, fcc and ω relative to hcp titanium. However, these values can be estimated using ab initio calculations. The ground state energy differences for bcc, fcc and ω relative to hcp titanium at 0 K from different works [1, 74,75,89,109–111] are compared in Table 4. These theoretically calculated ground state energy differences using ab initio calculations are considered in the present optimization. The transition temperatures associated with the metastable phases are not experimentally measured in the literature. The transition temperatures of $T_{\omega\text{-hcp}}$ and $T_{\omega\text{-bcc}}$ can be obtained by considering the pressure-temperature (P-T) phase diagram of pure titanium, ab initio calculations using the quasi-harmonic approximation (QHA) as well as the Debye model [74], and rapid quenching experiments [112]. The transition temperature of $T_{\omega\text{-hcp}}$ is preferred 186 K from Mei et al. [74] to the extrapolation of high-pressure ω-hcp phase boundary due to its large pressure hysteresis. The transition temperature $T_{\omega\text{-bcc}}$ is taken as 723 K from Mirzayev et al. [112], which has less uncertainty (15 K) than the extrapolation of the high-pressure ω-bcc phase boundary and the QHA calculations [74]. The transition temperature $T_{\text{fcc-liquid}}$ is calculated to be 900 K from the SGTE database [1], which is adopted in the present work.

Table 5Summary of the heat capacity of vanadium.

Temperature interval, K	Phase	Method	Purity of V, wt.%	Reference
50-300	bcc	Calorimetry	99.5	Anderson [118]
10–273	bcc	Adiabatic	99.5	Clusius et al.
10 2/0	DCC	calorimetry	55.0	[119]
200–350	bcc	Adiabatic	n/a	Bieganski and
200-330	DCC	calorimetry	11/ а	Stalinski [120]
1.5–15	bcc	Adiabatic	99.999	Ishikawa and
1.5–15	DCC		99.999	
1 5 40	1	calorimetry	00.7	Toth [121]
1.5–40	bcc	Adiabatic	99.7	Chernoplekov
		calorimetry		et al. [122]
80–1000	bcc	Laser-flash	99.999	Takahashi et al.
		calorimetry		[136]
273–1873	bcc	Drop calorimetry	Purest	Jaeger and
				Veenstra [137]
300-1250	bcc	Comparative	99.74	Beakley [138]
		calorimetry		
800-1100	bcc	Comparative	99.8	Knezek [139]
		calorimetry		
500–1900	bcc	Adiabatic	99.74	Fieldhouse and
000 1300	Dec	calorimetry	,,,,	Lang [140]
400–1100	bcc	Drop calorimetry	99.8	Golutvin and
400-1100	DCC	Drop calorinetry	99.6	
				Kozlovskaya
000 1000	t	A 41-1-41-	00.54	[141]
320–1800	bcc	Adiabatic	99.74	Kohlhaas et al.
		calorimetry		[57]
320–1800	bcc	Adiabatic	n/a	Braun et al. [142]
		calorimetry		
1000-1900	bcc	Induction heating	99.72	Filippov and
				Yurchak [143]
1200-1800	bcc	Electron	99.94	Peletskii et al.
		bombardment		[144]
		heating		
1400–1700	bcc	Levitation	99.9	Margrave [145]
1400-1700	DCC		99.9	Margrave [143]
000 1000	1	calorimetry	/	At1
900–1900	bcc	n/a	n/a	Arutyunov et al.
				[146]
350–900	bcc	Calorimetry	n/a	Chekhovskoi and
				Kalinkina [147]
293–1773	bcc	Graphic integration	99.82	Neimark et al.
		method		[148]
1500-2100	bcc	Pulse heating	99.9	Cezairliyan et al.
				[149]
297-2190	bcc	Drop calorimetry	99.94	Berezin and
				Chekhovskoi
				[150]
300–1100	bcc	Integrated	n/a	Kulish and
300-1100	DCC	· ·	11/ (1	
		measurement method		Filippov [151]
050 1700	t		00.0	n dt . d
350–1700	bcc	Adiabatic	99.9	Bendick and
		calorimetry		Pepperhoff [152]
300–1900	bcc	Millisecond pulse	99.8	Stanimirović
		calorimetry		et al. [153]
500-2173	bcc	Adiabatic heating	99.94	Chekhovskoii
				et al. [154]
200-2125	bcc	Assessment	n/a	Maglić [117]
2250-2800	liquid	Levitation	99.9	Treverton and
	1.	calorimetry		Margrave [67]
2084–2325	liquid	Induction heating	99.94	Berezin et al.
		and massive copper		[155]
		calorimeter		[100]
300 3800	bcc,	Levitation	99.9	Lin and Erobbass
300–2800			77.7	Lin and Frohberg
	liquid	calorimetry	- 1-	[156]
0.0000	bcc,	Mathematical	n/a	Thurnay [113]
0–3000		description		
	liquid	•		
0–3000 300–2700	liquid bcc,	Assessment	n/a	Smith [114]
		•	n/a	Smith [114]
	bcc,	•	n/a n/a	
300–2700	bcc, liquid	Assessment		
300–2700 0–3600	bcc, liquid bcc, liquid	Assessment Assessment	n/a	NIST-JANAF [46]
300–2700	bcc, liquid bcc, liquid bcc,	Assessment		
300–2700 0–3600	bcc, liquid bcc, liquid	Assessment Assessment	n/a	NIST-JANAF [46]

^b PAW-GGA: Projector Augmented-Wave method within the Generalized Gradient Approximation.

^c PBE-GGA: Becke-Perdew function within the Generalized Gradient Approximation.

Table 6

Debye temperature, Einstein temperature and electronic specific heat coefficient for different allotropes of vanadium.

Phase	$\theta_{\mathrm{D}}(-3)$, K	$\theta_{\rm D}(0),{\rm K}^{\rm a}$	θ E, K	γ , mJ/(mol·K)	Reference
bcc	366	344.04	245.64		Takahashi et al. [136]
	400	376.00	268.46	9.64	Shen [128]
	298	280.12	200.01	8.996	Corak et al. [123]
	308	289.52	206.72	8.996	Worley et al. [124]
	338	317.72	226.85	9.26	Corak et al. [125]
	315	296.10	211.42	8.87	Cheng et al. [126]
	391	367.54	262.42		Martin [157]
	399	375.06	267.79	9.92	Keesom and Radebaugh [127]
	345	324.30	231.55	9.247	Van Reuth [158]
	382	359.08	256.38	9.82	Radebaugh and Keesom [129]
	399	375.06	267.79	9.90	Heiniger et al. [159]
	399	375.06	267.79	9.9	Junod et al. [160]
	377	354.38	253.03	9.45	Corsan and Cook [161]
	423	397.62	283.90	9.63	Ishikawa [121]
	373	350.62	250.34	9.80	Chernopleko et al. [122]
	399	375.06	267.79		Sellers et al. [132]
	411	386.34	275.85	10.4	Kumagai and Ohtsuka [131]
	397.2	373.37	266.58	9.67	Leupold et al. [134]
	314	295.16	210.74	9.60	Pan et al. [162]
	357	335.58	239.60	9.47	Ohlendorf and Wicke [135]
	382	359.08	256.38	8.8	Vergara et al. [163]
	384	360.96	257.73	0.0	Guillermet and Grimvall [164]
	375.4	352.88	251.96		Iglesias-silva and Hall [165]
	380	357.20	255.04	9.26	Kittel [84]
	385 ± 5	361.90	258.40	9.75 ± 0.3	Desai [115]
	397.2	373.37	266.59	9.67	Arblaster [116]
	363.73	341.91	244.12	9.669	Li et al. [167]
	303.75	375	267.75	9.26	Tomilo [166]
		359	256.33	7.20	Chen and Sundman [85]
		337	292.60		Vřešt'ál et al. [110]
	396	372.24	265.78		This work (DFT)
	390	3/2.24	265.09	3.91 ^c	This work (CALPHAD)
hcp	414	389.16	277.86	9.889	Li et al. [167]
пер	414	389.10	318.78	9.009	Vřešt'ál et al. [110]
			283.11	2.89 ^c	This work (CALPHAD)
£aa	398	374.12	267.12	9.711	•
fcc	396	3/4.12	306.46	9./11	Li et al. [167]
				2.36°	Vřešťál et al. [110]
	344	323.36	266.97 230.88	2.30	This work (CALPHAD)
ω	344	343.30		2.20°	This work (CALDUAD)
1114	poo L pod	001 07	247.98	2.20	This work (CALPHAD)
liquid-amorphous	$299 \pm 29^{\rm d}$	281 ± 27	201 ± 19	0.000	Grimvall [96]
	232.9	218.93	156.31	9.929	Li et al. [167]
			202.79	3.75 ^c	This work (CALPHAD)

^a $\theta_D(0)$ is derived from 0.94- $\theta_D(-3)$ [78] when $\theta_D(0)$ is not available in the literature.

2.2. Pure vanadium

The stable solid state for vanadium is the bcc structure isotypic with W. Its atomic weight is 50.9415. The values of the heat capacity, enthalpy, enthalpies of transition and fusion, entropy, etc., for vanadium have been recommended by different authors [46,113–117]. The recommended values of heat capacity, enthalpy, entropy, and Gibbs energy function are covering a large temperature range of about 0–3800 K and they are in good agreement with each other. In order to facilitate reading, the thermodynamic properties of vanadium are reviewed and summarized in the present work.

The reported heat capacities of pure vanadium are summarized in Table 5. The low temperature heat capacity of bcc vanadium between 0 and 300 K was measured by several groups [118–122] using different calorimetric methods. Their experimental results are in agreement with each other within the experimental error. The recommended values of heat capacity between 0 and 300 K from NIST-JANAF edited by Chase [46], Desai [115] and Arblaster [116] agree well with the experimental data with the deviations of about $\pm 3\%$ below 15 K, $\pm 10\%$ from 15 to 150 K, and $\pm 3\%$ from 150 to 298.15 K. The superconducting state and its transition temperature $T_{\rm c}$ for vanadium between 0 and 5.5 K have been

experimentally investigated by many researchers [121,123-135] and reviewed by Desai [115] and Arblaster [116]. The superconducting transition temperature was recommended to be 5.4 \pm 0.3 K by Desai [115] and 5.435 K by Arblaster [116]. The superconducting state of vanadium is not considered in the present work and its details can be found elsewhere [115,116]. The high temperature heat capacity of bcc vanadium in the temperature range from room temperature to melting point has been experimentally measured in different works [57, 136-153]. The measured results are in a general consistency except for the data from Beakley [138], Golutvin and Kozlovskaya [141], Margrave [145], and Bendick and Pepperhoff [152]. The values from Beakley [138] and Golutvin and Kozlovskaya [141] are high scattered and relatively large, and the values from Margrave [145] and Bendick and Pepperhoff [152] are relatively small. Chekhovskoii et al. [154] investigated the contribution of equilibrium vacancies to the caloric properties of vanadium on the basis of the average heat capacities. The measured average heat capacities of pure vanadium by Chekhovskoii et al. [154] are much lower than the reported heat capacities from other works. Thus, the measured heat capacities of bcc vanadium from the works [138,141,145,152,154] are not accepted in the present optimization. Based on the experimental heat capacity of bcc vanadium

^b $\theta_{\rm E}$ is derived from 0.714- $\theta_{\rm D}$ (0) [76].

 $^{^{\}rm c}$ The optimized value for a in Eq. (4), which consists of electronic excitations and low-order anharmonic vibrational contributions (dilatational and explicitly anharmonic).

 $^{^{}m d}$ $\theta_{
m D}$ (-3) of amorphous state is lower by 15–30% of the one of crystalline state, which was assumed by Grimvall [96].

Table 7Summary of the enthalpy, entropy and melting point of vanadium.

$\Delta_{\rm fus} H^{\rm o}$, J/mol	$H^{o}(298.15 \text{ K})-H^{o}(0 \text{ K}), \text{ J/mol}$	S°(298.15 K), J/ (mol·K)	$\Delta_{\rm fus}S^{\rm o}$, J/ (mol·K)	Melting point, K	Method	Reference
17312 ± 712			7.953 ± 0.335	2175	Levitation calorimetery	Treverton and Margrave [67]
18180				2179	Levitation calorimetry	Margrave [145]
23037				2190 ± 10	Drop calorimetry	Berezin and Chekhovskoi [150]
21905				2190	Pulse heating	Gathers et al. [168]
27508					Pulse heating	Seydel et al. [169]
23036				2202	Levitation calorimetry	Lin and Frohberg [156]
23000				2190	Mathematical description	Thurnay [113]
				2199 ± 6	DTA	Rudy and Windisch [172]
				2200	Six-wavelength	Hiernaut [173]
					pyrometer	
				2201	Pulse heating	McClure and Cezairlliyan
						[174]
				2199	Pulse heating	Pottlacher et al. [171]
				2220	Adiabatic heating	Chekhovskoii et al. [154]
20937	4640	28.911 ± 0.4		2199	Assessment	Hultgren et al. [65]
	4580	28.67			Assessment	Glushko et al. [66]
21500 ± 3000	4707 ± 50	30.89 ± 0.30	9.9 ± 1.0	2183	Assessment	Smith [114]
22840 ± 6280	4640	28.936 ± 0.42	10.432	2190 ± 20	Assessment	NIST-JANAF [46]
21000 ± 2500	4707 ± 10	29.708 ± 0.08	9.537 ± 1.2	2202	Assessment	Desai [115]
23023 ± 400	4678	29.64	10.4607	2201 ± 6	Assessment	Arblaster [116]
21500	4507	30.89	9.8488	2183	CALPHAD	SGTE [1]
21023	4706	29.85	9.5474	2202	CALPHAD	This work

available in the literature, NIST-JANAF [46], Desai [115] and Arblaster [116] recommended the values of heat capacity and provided the deviation between experiments and recommended values to be about $\pm 2\%$ from 298.15 to 1000 K and $\pm 3\%$ from 1000 K to the melting point. The heat capacities of bcc vanadium recommended by NIST-JANAF [46], Desai [115] and Arblaster [116] are consistent with each other and adopted to evaluate the model parameters in the present work. The heat capacity of the liquid vanadium has been experimentally investigated in several works [67,155,156]. The measured heat capacity of liquid vanadium to be 48.744 J/(mol·K) by Treverton and Margrave [67] is larger than the values 46.191 and 46.72 J/(mol·K) from Berezin et al. [155] and Lin and Frohberg [156], respectively. The heat capacity of liquid was also calculated by Thurnay [113] to be 46.72 J/(mol·K) based on the measured oen from Lin and Frohberg [156]. Smith [114], NIST-JANAF [46], Desai [115] and Arblaster [116] recommended the values of the heat capacity of liquid vanadium based on the data from the works [67,155,156]. The recommended values [46,115,116] and experimental data [155,156] of the liquid heat capacity are adopted in the present optimization due to their consistency. For the metastable hcp, fcc and ω vanadium, neither experimental measurement nor theoretical calculation of heat capacities have been reported in the literature.

Chen and Sundman [78] reported the value of ratio $\theta_D(0)/\theta_D(-3)$ for bcc vanadium to be 0.94, which is assumed the same for hcp, fcc, ω and liquid-amorphous vanadium. The Debye temperatures $\theta_D(-3)$ and $\theta_D(0)$, Einstein temperature $\theta_{\rm E}$, and electronic specific heat coefficient γ for different allotropes of vanadium are summarized in Table 6. The low temperature limit of the Debye temperature $\theta_D(-3)$ for bcc vanadium has been studied by many researchers [84,121-129,131,132,134-136, 157-165]. Most of their values are consistent with each other except for some larger values [121,131] and smaller values [123-126,158,162]. Desai [115] recommended the value of θ_D (-3) for bcc vanadium to be 385 ± 5 K based on a large number of experimental data [121–129,131, 132,134–136,157,160–163]. While Arblaster [116] suggested the value of θ_D (-3) to be 397.2 K adopted from Leupold et al. [134] because of the very high purity of the samples used. The high temperature entropy Debye temperature $\theta_D(0)$ and Einstein temperature θ_E for bcc vanadium in Table 6 are derived from the relations $\theta_D(0) = 0.94\theta_D(-3)$ [78] and θ_E = 0.714 θ_D (0) [76], respectively. The difference between θ_E values obtained from the Debye temperature recommended by Desai [115] and Arblaster [116] is only about 8 K. Here, it is believed that the recommended values by Desai [115] and Arblaster [116] are acceptable. In addition, Tomilo [166] as well as Chen and Sundman [85] reported the

Debye temperatures $\theta_D(0)$ to be 375 and 359 K, respectively, which are consistent with the values derived from $0.94 \cdot \theta_D(-3)$. For the hcp, fcc, ω and liquid vanadium, their Debye and Einstein temperatures have been rarely reported in the literature. Li et al. [167] assessed the experimental heat capacities of the stable bcc and liquid phases of vanadium from 0 to 298.15 K using the polynomial and Debye model, and extrapolated the heat capacities of the metastable hcp and fcc vanadium by the Debye model. The Debye temperature $\theta_D(-3)$ and electronic specific heat coefficient γ for the bcc, hcp fcc and liquid phases were obtained via the polynomial model by fitting the data of heat capacity [167]. Vřešťál et al. [110] obtained the Einstein temperatures of bcc, hcp and fcc V by extending the SGTE Gibbs energy expression to 0 K based on the Einstein formula. The Einstein temperatures from Vřešt'ál et al. [110] are slightly larger than the corresponding values from other works [85,115,116, 167]. Thus, the Debye and Einstein temperatures for the metastable hcp and fcc vanadium from Li et al. [167] are considered in the present work. The Debye temperature for the ω vanadium is not available in the literature, which is computed by the ab initio calculations in the present work. The Debye temperatures of the liquid-amorphous phase for vanadium and related systems are also not reported in the literature. As mentioned above, the Debye temperature of liquid-amorphous vanadium can be predicted according to the assumption from Grimvall [96], where the Debye temperature of amorphous vanadium is lower by 15–30% of the one of bcc vanadium. Since this assumption was found to be valid for titanium, the predicted Debye temperature for liquid-amorphous vanadium is adopted in the present work.

The enthalpies and entropies of fusion for vanadium are summarized in Table 7. The enthalpy of fusion $\Delta_{fus}H^{o}$ for vanadium was experimentally measured by many research works [67,113,145,150,156,168, 169] through different methods. Smith [114], NIST-JANAF [46] and Desai [115] recommended the values of $\Delta_{fus}H^{o}$ for vanadium to be 21500 ± 3000 , 22840 ± 6280 and 21000 ± 2500 J/mol, respectively, based on the available experimental data [67,145,150,156,168,169], and Arblaster [116] recommended the value to be 23023 \pm 400 J/mol, which is the average of the experimental data from Berezin and Chekhovskoi [150] and Lin and Frohberg [156]. The experimental results and recommended values are consistent to some extent and they are adopted in the present work. The values of Ho(298.15 K)-Ho(0 K) and $S^{o}(298.15 \text{ K})$ for vanadium were recommended in several works [46,65, 66,114–116] on the basis of the values for heat capacity C_p and the quantity C_p/T , respectively. The entropy of fusion $\Delta_{\text{fus}}S^0$ was also recommended by integration of C_p/T and $S^0(298.15 \text{ K})$. These

Table 8 The ground state energy differences for hcp, fcc and ω relative to bcc vanadium at 0 K from DFT calculations and CALPHAD approach.

$\Delta E_{\text{hcp-bcc}}$, J/mol	$\Delta E_{ m fcc-bcc}$ J/mol	$\Delta E_{\omega ext{-bcc}}$, J/mol	Method	Reference
24478	23948		PAW-GGA	Wang et al. [109]
3894	7478	12655	Extrapolation based on Einstein model QE-USPP ^a	Vřešťál et al. [110] Yan and Olson [88]
		8965	CALPHAD	Yan and Olson [88]
25183	24893		DFT	OQMD [111]
4000	7500		CALPHAD	SGTE [1]
24801	23672	11998	DFT	This work
4000	7500	6997	CALPHAD	This work

^a QE-USPP: Quantum Espresso with the Ultra-Soft Pseudopotentials.

recommended values are accepted in the present work since they are consistent with each other. In addition, $H_m(T)-H_m(298.15\,K)$ and $S_m(T)-S_m(298.15\,K)$ of pure vanadium were experimentally investigated by many groups of researchers [67,113,136,150,154–156,168, 170,171]. Their experimental results are consistent with the recommended values [46,115,116] except the values from Gathers et al. [168]. The experimental data from Gathers et al. [168] are much larger than the values from the other authors when the temperature is above 2500 K. Thus, the data from Gathers et al. [168] are not used in the present work.

The measured and recommended melting points for vanadium are also summarized in Table 7. The melting point of vanadium has been experimentally studied by a large number of researchers [67,145,150, 154-156,168,171-174]. There is a slight discrepancy among these experimental data. The melting point of vanadium (2183 K) was adopted widely in the first and second generation thermodynamic database [1] based on the recommended value from Smith [114], which is the average values of 2175 K [67], 2179 K [145], 2190 \pm 10 K [150] and 2190 K [168]. However, a higher melting point (2199-2220 K) was measured in some other works [156,171-174]. Desai [115] recommended the melting point of vanadium to be 2202 K proposed by Hultgren et al. [65], and Arblaster [116] suggested it to be 2201 \pm 6 K based on the experimental data from Rudy and Windisch [172], Hiernaut [173] and Pottlacher et al. [154,171]. In the present work, the value 2202 K for the melting point of vanadium is adopted according to the recommended values from Desai [115] and Arblaster [116].

The ground state energy differences for the hcp, fcc and ω phases relative to bcc vanadium at 0 K from *ab initio* calculations and CALPHAD approach [1,88,109–111] are compared in Table 8. The values of $\Delta E_{\text{hcp-bcc}}$ and $\Delta E_{\text{fcc-bcc}}$ from Wang et al. [109] and OQMD database [111] calculated using DFT are consistent, however, they are larger than the values from Vřešt'ál et al. [110] and SGTE database [1]. Similar observation has been found for the $\Delta E_{\omega\text{-bcc}}$ value. These calculated ground state energy differences are considered during the optimization of model parameters. The transition temperatures $T_{\text{hcp-liquid}}$ and $T_{\text{fcc-liquid}}$ are calculated from the SGTE database [1] to be 1414 and 1189 K, respectively, which are adopted in the present work.

2.3. The Ti-V system

The phase equilibria of the Ti–V binary system are rather simple due to the presence of only three phases, i.e. liquid, (β Ti, V) and (α Ti). Several versions of thermodynamic description for the Ti–V system based on the SGTE database [1] are available in the literature [175–178]. Murray [179,180] had critically reviewed the phase equilibria of this system. Two types of phase diagrams for the Ti–V system have been reported. One is characterized by a miscibility gap in the (β Ti, V) phase with a critical temperature at 1123 K, giving rise to a

monotectoid reaction $(\beta Ti) \to (\alpha Ti) + (V)$ at 948 K, which is based on the work of Nakano et al. [181]. However, the new experimental results from Fuming and Fowler [182] showed that no evidence has been obtained for the existence of the miscibility gap. Instead, a stable $(\alpha Ti) + (\beta Ti, V)$ two-phase region was observed in the high-purity samples. The miscibility gap is promoted by the increase of oxygen content in the Ti–V alloys. Thus, the reported miscibility gap by Nakano et al. [181] is possibly due to the oxygen contamination. Another type is characterized by a continuously decreasing $(\beta Ti, V)/(\alpha Ti) + (\beta Ti, V)$ transus with the increase of vanadium concentration without a miscibility gap nor a monotectoid reaction, which is widely accepted in the literature.

The liquidus of the Ti-V system has not been measured experimentally yet. The solidus was determined by Adenstedt et al. [183] and Rudy [184]. The liquidus and solidus have a congruent minimum at about 35 at.% V and 1877 \pm 5 K [184]. The phase boundaries of $(\alpha Ti)/(\alpha Ti)$ + (βTi , V) and (βTi , V)/(αTi) + (βTi , V) as well as the phase regions of (αTi) , $(\alpha Ti) + (\beta Ti, V)$ and $(\beta Ti, V)$ were determined by several group of researchers [183,185-189]. The results showed that the solubility of V in (αTi) increases first and then decreases with the increase of temperature and its maximum value is about 3.7 at.% around 773-873 K. The phase boundary (βTi , V)/(αTi) + (βTi , V) decreases continuously with the increase of vanadium content. Rolinski et al. [190] determined the activity of solid Ti-V alloys by the Knudsen effusion method combined with a mass spectrometer sensing technique. Mill and Kinoshita [191] measured the activity of Ti and V in the liquid Ti-V alloys by a technique involving electromagnetic levitation in an inert atmosphere. The results showed a slight positive deviation from the Raoult's law in the liquid Ti-V alloys, which are consistent with the activity measurements for solid Ti-V alloys reported by Rolinski et al. [190].

In addition to the experimental investigation of the Ti–V system, theoretical studies were adopted to study the enthalpy of solution [192] and phase equilibria [193]. The enthalpies for both pure Ti and V as well as solid solution alloys (hcp-Ti $_{35}$ V $_{1}$, hcp-Ti $_{1}$ V $_{35}$, bcc-Ti $_{26}$ V $_{1}$ and bcc-Ti $_{1}$ V $_{26}$, in at.%) were calculated by Uesugi et al. [192] using *ab initio* calculations. The enthalpies of the hcp phase increased with the increasing of V concentration, while the enthalpies of the bcc phase decreased. The subsolidus equilibrium phase diagram of the Ti–V system has been computed by Chinnappan et al. [193] through cluster expansion, lattice dynamics and Monte Carlo modeling methods combined with DFT calculations. The computed phase boundaries are in good agreement with the assessed boundaries using the CALPHAD method.

2.4. The metastable phases in the Ti-V system

Although the phase equilibria of the Ti-V system are simple, the phase transformations in this system are complex due to the existence of metastable phases. As mentioned above, two types of martensite namely α' and α'' , and metastable ω phase may coexist in the Ti–V alloys depending on the V concentration. One of the earliest study on asquenched and aged Ti-V alloys was conducted by McCabe et al. [194] using high-resolution dark-field microscopy and selected-area diffraction. The experimental results indicated that the morphology of the ω phase of alloys aged for a short time was similar to that of the as-quenched alloys. Leibovitch et al. [195] investigated a series of as-quenched Ti-V alloys by transmission electron microscopy (TEM) along with X-ray diffraction (XRD) analysis and reported that the stability range of the single α' , $\alpha' + \beta + \omega$, $\beta + \omega$, and single β is 0–8 at.%, 8-14 at.%, 14-25 at.%, and 25-100 at.% V, respectively. Ming et al. [196] investigated pressure-induced ω phase formation in polycrystalline Ti-V alloys up to 25 GPa at ambient temperature using a diamond anvil pressure cell and XRD techniques. It was found that the $\boldsymbol{\omega}$ phase was more stable under high pressure conditions than the α and β phases for alloys with less than 30 at. % V and no ω phase was detected for alloys with higher than 30 at.% V. The phases were identified as α' for 0–8.5 at. % V, α' + β for 8.5–10.4 at. % V, α' + β + α'' + ω for 10.4–14.2 at. % V, $\beta + \omega$ for 14.2–24.8 at. % V, and single-phase β for

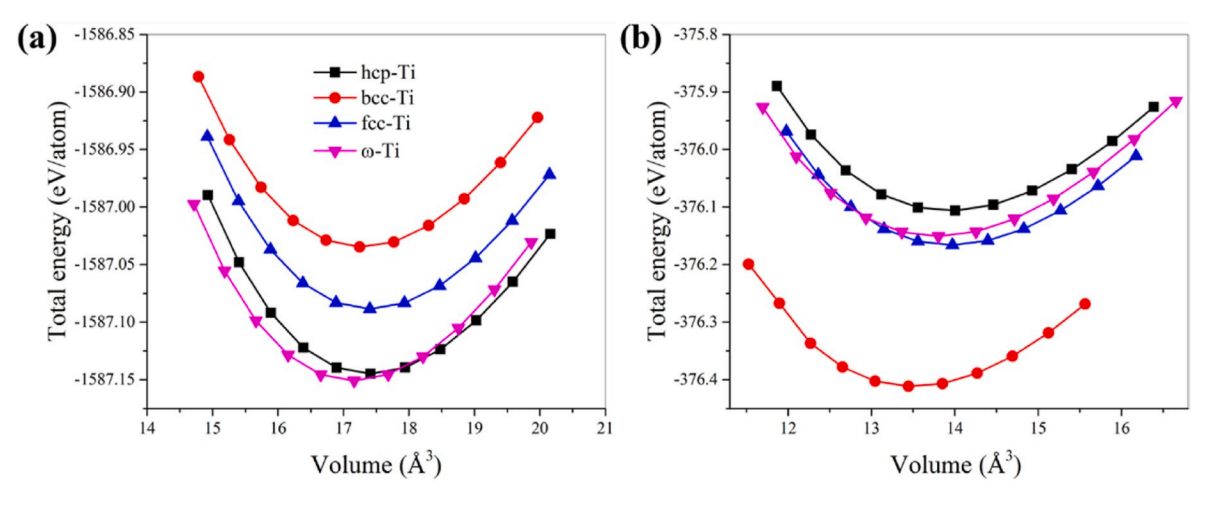


Fig. 1. Total energy as function of volume for the stable and metastable allotropes of (a) titanium and (b) vanadium obtained using DFT calculations.

Table 9Summary of DFT calculations results for different allotropes of titanium and vanadium.

Element	Phase	Space group	Pearson symbol	ΔE (J/mol)	Reference stae	Lattice paramete	ers (Å)
						Initial	Optimized
Ti	hcp	P6 ₃ /mmc	hP2	0	hcp	a = 2.939	a = 2.933
						c = 4.641	c = 4.657
	ω	P6/mmm	hP3	-571		a = 4.577	a = 4.572
						c = 2.829	c = 2.828
	bcc	Im3m	cI2	+10619		a = 3.252	a = 3.259
	fcc	Fm3m	cF4	+5438		a = 4.109	a = 4.115
v	bcc	Im 3 m	cI2	0	bcc	a = 2.993	a = 3.000
	ω	P6/mmm	hP3	+11998		_	a = 4.256
		·					c = 2.631
	hcp	P6 ₃ /mmc	hP2	+24801		_	a = 2.742
	=	• •					c = 4.325
	fcc	Fm3m	cF4	+23672		a = 3.819	a = 3.817

Table 10
Calculated independent elastic constants (in GPa) for different allotropes of titanium and vanadium using the ElaStic code.

Element	Phase	C ₁₁	C ₁₂	C ₄₄	C ₁₃	C ₃₃
Ti	hcp	169	95.1	42.4	75.7	192.9
	ω	199.1	85.3	55.1	50.3	253.1
	bcc ^a	88.8	117.2	34.6	-	_
	fcc	133.5	97.8	61.5		-
V	bcc	268.2	141.8	12.7		-
	ω	296.2	138.1	10.7	138.1	266.3
	hcp ^a	-454.8	510.7	307.5	241.8	-114.6
	fcca	3.8	269.2	5.6	-	_

^a Dynamically unstable structures.

Table 11Computed elastic properties and Debye temperatures for different allotropes of titanium and vanadium using the ElaStic code.

Element	Phase	E (GPa)	B (GPa)	G (GPa)	ν	θ_D (K)
Ti	hcp	113.93	113.76	42.73	0.33	397
	ω	159.18	113.62	62.84	0.27	475
	fcc	101.16	109.66	37.57	0.35	371
	bcca	-132.6	107.76	-38.9	0.71	-
V	bcc	73.87	183.97	25.77	0.43	396
	ω	137.02	187.23	35.88	0.41	344
	hcp ^a	150.86	287.69	-104.1	0.82	-
	fcca	-62.49	180.75	-20.06	0.56	-

^a Dynamically unstable structures.

composition higher than 24.8 at. % V from XRD patterns of the Ti–V alloys quenched after solution treatment by Matsumoto et al. [197]. Dobromyslov and Elkin [198] reported that the minimum concentration of V for the formation of $\alpha^{\prime\prime}$ phase in the quenched Ti–V alloys was 9.0 at. % determined using XRD and TEM. Moreover, the structural properties, morphology and transformation/precipitation mechanism for the metastable phases in the Ti–V alloys have also been studied by many researchers [29,199–201] using different characterization methods, such as XRD, SEM, neutron diffraction, TEM, atom probe tomography (APT).

The martensite start temperatures (M_s) and the ω start temperatures (ω_s) for the Ti–V system have been experimentally studied by several researchers [202–213]. Additionally, the martensite and ω formation has been studied theoretically [88,214-216]. The M_s and ω_s temperatures decrease with the increase of the alloying element V. The reported experimental values for the M_s temperature are relatively consistent with each other, whereas the ω_s temperatures scatter noticeably. It may be due to the influence of oxygen content on the $\beta \to \omega$ transformation, which has been studied by Paton and Williams [211]. The experimental results show that the increase of the oxygen content significantly reduces the ω_s start temperature. Recently, the $\beta\text{--}\alpha'/\alpha''$ martensitic transformation and ω formation for the Ti-V system have been thermodynamically described by Yan and Olson [88], Hu et al. [217] and Lindwall et al. [178] using the CALPHAD approach based on the SGTE database [1]. The T_0 curves (the temperature where the Gibbs free energy difference of two phases is equal to zero) between β and α , $T_0(\beta/\alpha)$, and between β and ω , $T_0(\beta/\omega)$, have also been calculated. However, the calculated solubilities of V in the (αTi) phase by Yan and Olson [88] and

Table 12Summary of the Gibbs energy expressions for titanium.

Phase	Gibbs energy expressions, J/mol	Temperature range, K
hcp	$GTIHCPL = -8187.11746 - 3.88479749E - 03T^2 - 1.12754876E - 14T^5$	0–1941
	GTIHCPH = -34429.8962 + 168.6069891T - 21.5018141Tln(T)	1941–6000
	-1.53262730 E $+18T^{-5}$ $+8.83870501$ E $+37T^{-11}$	
	THETA(HCPTI) = LN(269.66)	0–6000
bcc	$GTIBCCL = -1189.30591 - 1.75640865E - 03T^2 - 2.11276133E - 14T^5$	0–1941
	$ GTIBCCH = -38328.0689 + 179.0443615T - 21.6601815T \ln(T) + 2.08872908E + 19T^{-5} - 6.22559747E + 37T^{-11} + 1000000000000000000000000000000000$	1941–6000
	THETA(BCCTI) = LN(192.01)	0–6000
fcc	$GTIFCCL = -1308.28194 - 1.10005324E - 03T^2 - 4.82225830E - 14T^5$	0-1941
	$GTIFCCH = -34080.2880 + 176.8506164T - 21.5028284T \ln(T)$	1941–6000
	$-1.09974048E + 18T^{-5} + 9.00001480E + 37T^{-11}$	
	THETA(FCCTI) = LN(236.67)	0–6000
ω	$GTIOMEL = -8646.04379 - 1.75612531E - 03T^2 - 3.77858605E - 14T^5$	0–1941
	$GTIOMEH = -40191.3391 + 175.1217992T - 21.5072012T \ln(T)$	1941–6000
	$-1.00203889E + 18T^{-5} + 9.79952638E + 37T^{-11}$	
	THETA(OMETI) = LN(289.30)	0–6000
liquid-amorphous	$GTILIQ = +4349.70025 - 2.00294843E - 03T^{2}$	0–6000
	THETA(LIQTI) = LN(185.76)	0–6000
	GD(LIQTI) = +49395.4110-8.314T-0.737261354Tln(T)	0–6000

THETA = $1.5R\theta_E + 3RT \ln[1 - \exp(-\theta_E/T)]$; GD = $-RT \ln[1 + \exp(-\Delta G/RT)]$

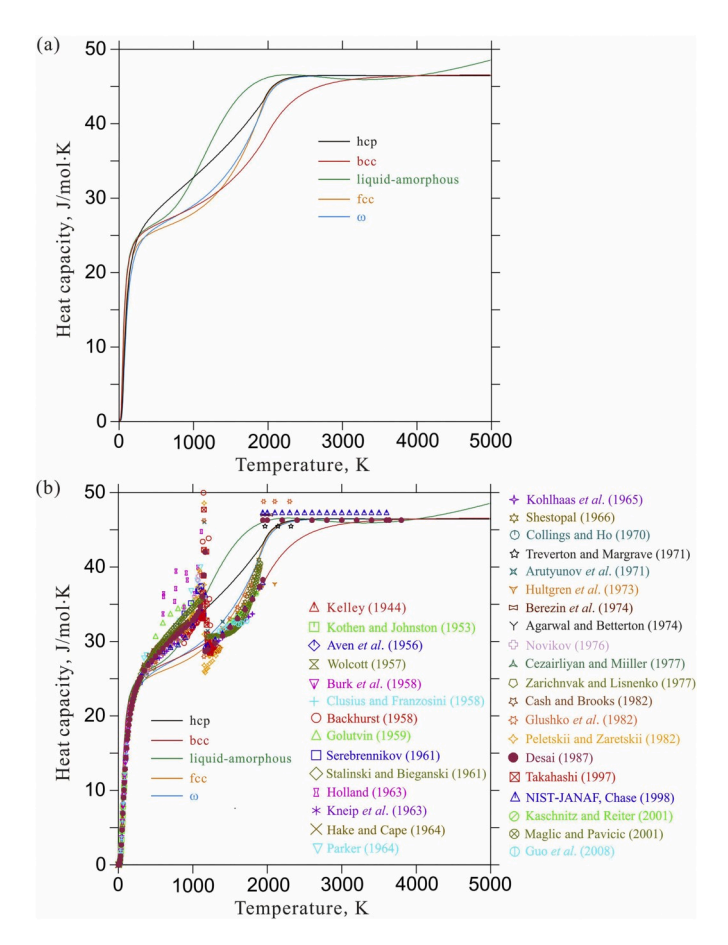


Fig. 2. (a) Calculated heat capacities of different allotropes for titanium and (b) comparison between the calculated and experimental heat capacities of titanium.

Hu et al. [217] are smaller than the reported values in the literature and the calculated $T_0(\beta/\alpha)$ curve by Lindwall et al. [178] is larger than the experimentally measured data. Thus, the Ti–V system is reassessed based on the new lattice stabilities of Ti and V in order to improve the thermodynamic description of martensitic transformation and ω phase transition in the Ti–V alloys.

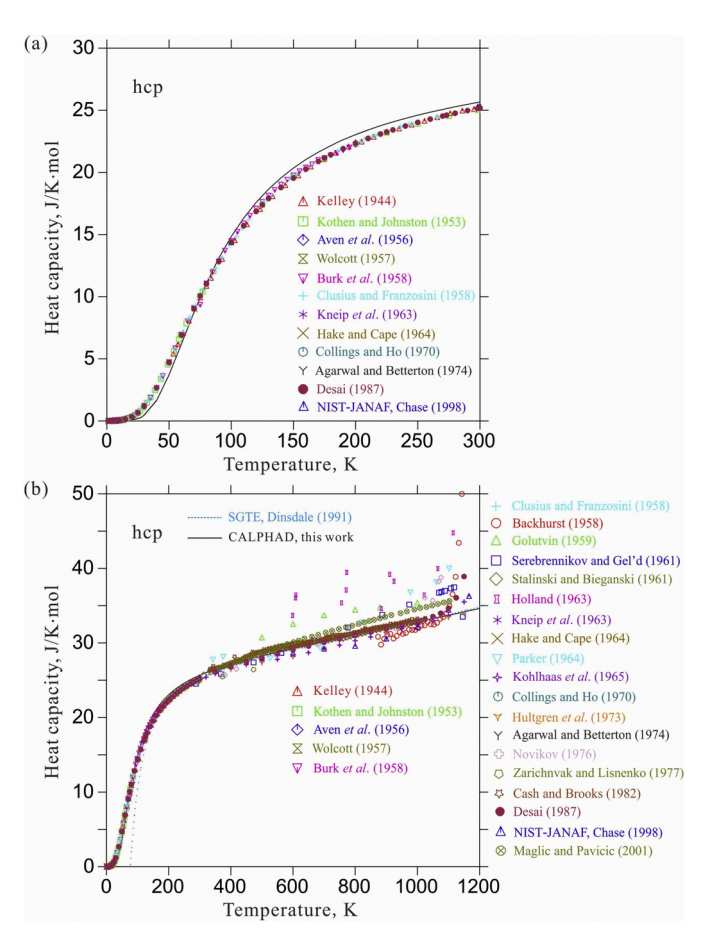


Fig. 3. Calculated heat capacities of hcp titanium (a) below room temperature and (b) below 1200 K in comparison with the experimental data and SGTE database [1].

3. Methodology

3.1. Ab initio calculations

The total energies of the stable and metastable allotropes of titanium and vanadium were calculated using *ab initio* calculations based on DFT [218,219] as implemented in the Quantum Espresso (QE) package

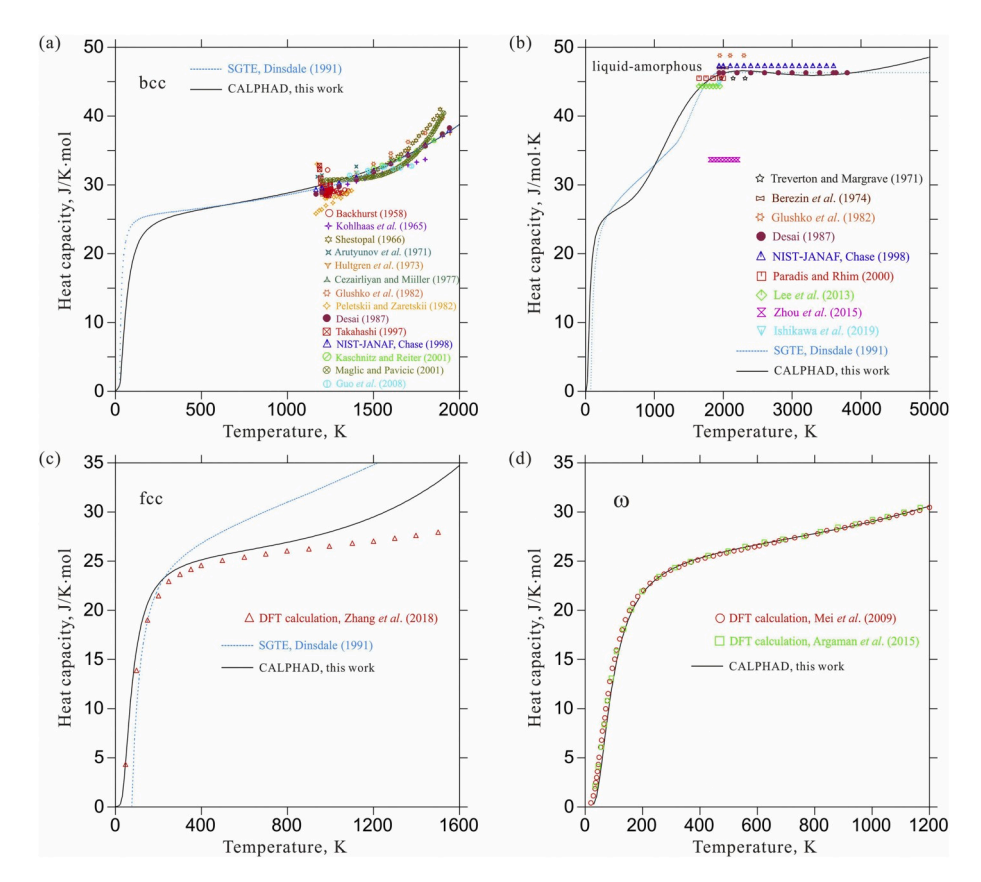


Fig. 4. Calculated heat capacities of (a) bcc, (b) liquid-amorphous, (c) fcc, and (d) ω titanium in comparison with experimental data and SGTE database [1].

[220]. QE is a self-consistent pseudopotential code with numerical plane waves as the basis set for decomposition of the one-electron wavefunctions. Ultrasoft pseudopotentials developed by Vanderbilt [221] were used to describe the interaction between the valence electron and the ionic core. A generalized gradient approximation proposed by Perdew-Becke-Ernzerhof (GGA-PBE) [222] was employed as the exchange-correlation functional and the k-points in the Brillouin zone were sampled using the Monkhorst-Pack scheme [223]. The kinetic energy cutoff for the wavefunction was set to be 45 Ry and an energy cutoff of 360 Ry is used for charge density and potential. The k-point spacing was maintained to be $< 0.02 \text{ Å}^{-1}$ in each direction for all the structures. The kinetic energy cutoff and the number of k-points were chosen such that the total energy was converged within 10^{-4} Ry/atom. Methfessel-Paxton smearing scheme [224] with a smearing width of 0.02 Ry was used to account for the occupancies. The volume, shape and atomic positions of all the structures were relaxed using the Broyden-Fletcher-Goldfarb-Shanno (BFGS) algorithm [225] until the energy was converged to 10^{-7} Ry in each electronic step and the force was converged to 10^{-3} Ry/bohr³ in each ionic step during the geometric optimization.

The equilibrium structures with the minimum energy obtained from the DFT calculations were used as input to obtain the elastic constants for the stable and metastable allotropes of Ti and V. The independent elastic constants and elastic properties for each structure were calculated using the ElaStic code [226]. Eleven distorted structures were generated for each strain with a maximum Lagrangian strain of 0.03. The total energy of each deformed structure was calculated using QE and the computed energies are fitted to a polynomial function of the applied strain for calculating the derivatives at zero strain. From these results, the elastic constants C_{ij} were calculated from which other elastic properties such as Young's modulus (E), shear modulus (G), bulk modulus (B) and Poisson's ratio (ν) can be derived. From the elastic properties computed using the ElaStic code, the Debye temperature (θ_D) for each

allotrope was calculated using the following equations proposed by Andersson [227].

$$\theta_D = \frac{h}{k} \left[\frac{3n}{4\pi} \left(\frac{N_A \rho}{M} \right) \right]^{1/3} v_m \tag{1}$$

$$v_m = \left[\frac{1}{3} \left(\frac{2}{v_i^3} + \frac{1}{v_i^3}\right)\right]^{-1/3} \tag{2}$$

$$v_{l} = \left(\frac{G}{\rho}\right)^{1/2} \text{ and } v_{l} = \left(\frac{3B + 4G}{3\rho}\right)^{1/2}$$
 (3)

where, h is the Planck's constant, k is the Boltzmann constant, n is the number of atoms, N_A is the Avagadro's number, ρ is the density, M is the molecular weight, ν_m is the mean velocity, ν_t is the transverse velocity of sound and ν_t is the longitudinal velocity.

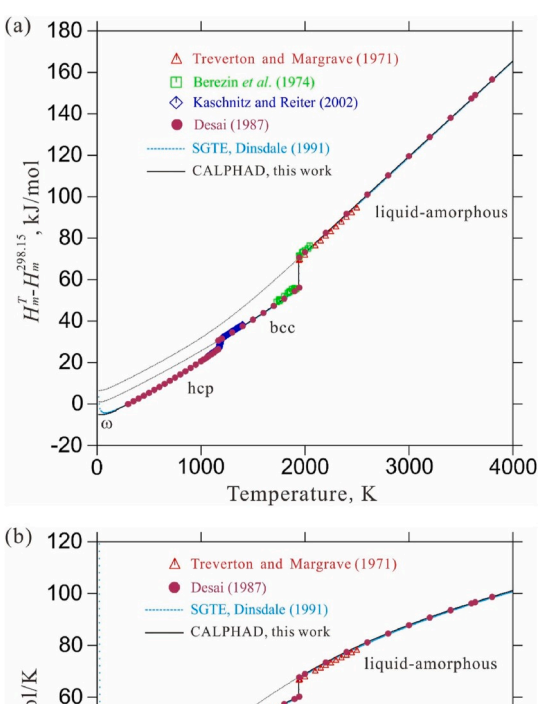
3.2. Thermodynamic modeling

3.2.1. Pure elements

3.2.1.1. Solid phases. In the third generation thermodynamic database, the new thermodynamic model with Einstein function for description of pure element has been developed by Chen and Sundman [6]. According to Chen and Sundman, the heat capacity of solid phases in the temperature range below the melting point can be expressed as follows:

$$C_{p} = 3R \left(\frac{\theta_{E}}{T}\right)^{2} \frac{e^{\theta_{E}/T}}{\left(e^{\theta_{E}/T} - 1\right)^{2}} + aT + bT^{4} + C_{p}^{mag}$$
(4)

in which the first term is the contribution from the harmonic lattice vibration, R is gas constant, and θ_E is the Einstein temperature. aT represents the contributions from the electronic excitations and low-order



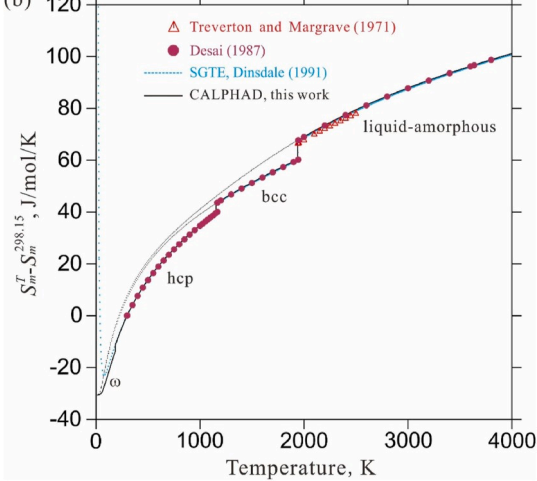


Fig. 5. Calculated the increments of (a) enthalpy $H_m(T) - H_m(298.15 \, K)$ and (b) entropy $S_m(T) - S_m(298.15 \, K)$ of titanium in comparison with experimental data, recommended values and SGTE database [1].

anharmonic corrections, and the parameter a is related to non-thermodynamic information, such as the electron density of states at the Fermi level. bT^4 indicates the contribution from the high-order anharmonic lattice vibration, and the parameter b can be hardly validated by experimental information. C_p^{mag} is the magnetic contribution. For titanium and vanadium, C_p^{mag} is zero since they do not show any magnetic ordering. Therefore, the following expressions will not include the magnetic contribution term.

The corresponding Gibbs energy can be derived from the expression of C_p in Eq. (4):

$$G = E_0 + \frac{3}{2}R\theta_E + 3RT \ln\left[1 - \exp\left(-\frac{\theta_E}{T}\right)\right] - \frac{a}{2}T^2 - \frac{b}{20}T^5$$
 (5)

where E_0 is the cohesive energy (i.e. total energy excluding the vibrational contribution) at 0 K, and the second and third terms are the energy of zero-point lattice vibration described by the Einstein model. These parameters E_0 , θ_E , a and b are used to fit the experimental heat capacity and enthalpy data from 0 K up to the melting point T_m .

The Gibbs energy for solid phases beyond the melting point should also be given a similar expression that results in the continuous curves for heat capacity, enthalpy and entropy at the melting point. The model needs to avoid a kink [228] in the heat capacity curve that is inherent in the direct extrapolation of the Gibbs energy for a solid phase over its melting point. The expressions of the heat capacity and Gibbs energy

above the melting point suggested by Chen and Sundman [6] are also adopted in the present work, as shown in Eqs. (6) and (7):

$$C_{p} = 3R \left(\frac{\theta_{E}}{T}\right)^{2} \frac{e^{\theta_{E}/T}}{\left(e^{\theta_{E}/T} - 1\right)^{2}} + a' + b'T^{-6} + c'T^{-12}$$
(6)

$$G = \frac{3}{2}R\theta_E + 3RT \ln\left[1 - \exp\left(-\frac{\theta_E}{T}\right)\right] + H' - S'T + a'T(1 - \ln T) - \frac{b'}{30}T^{-5} - \frac{c'}{132}T^{-11}$$
(7)

where a', b', and c' are optimized by assuming that, on the one hand, the heat capacity and its first derivative should have identical values at the melting point in Eqs. (5) and (7), and on the other hand, the heat capacity calculated from Eq. (6) should equal to the value for the liquid phase at an arbitrarily high temperature much beyond the melting point, e.g., 4000 K. The coefficients H' and S' are calculated from the enthalpy and entropy at the melting point, respectively. Eqs. (6) and (7) ensure that solid phase will not become stable again at very high temperatures and keep the continuity in both the heat capacity and its first derivative at the melting temperature. Recently, a new method, named the EEC (Equal-Entropy Criterion), was proposed by Sundman et al. [229] to prevent solid phases to become stable again when extrapolated to temperatures far above their melting temperature. It is very useful to detect the extrapolations that are nonphysical. However, this new method is still being developed. In the present work, the models proposed by Chen and Sundman [6] are sufficient enough to thermodynamically describe the low-temperature ω phase under the background of the third generation CALPHAD database.

3.2.1.2. Liquid-amorphous phases. The generalized two-state model proposed by Ågren [3,230] has been used to describe the liquid and amorphous phases, which were treated as one phase in which the atoms can be in either the liquid-like state or amorphous-like state. Thus, the liquid and amorphous phases are simply named the liquid-amorphous phase in the present work. With this model, the continuous change of thermodynamic properties, i.e. heat capacity, enthalpy and entropy, can be obtained from low temperature amorphous phase to high temperature liquid phase. According to Ågren [3,230], the Gibbs energy of the liquid-amorphous phase can be described by the following equation:

$$G^{liq-am} = {}^{\circ}G^{am} - RT \ln[1 + \exp(-\Delta G_d/RT)]$$
(8)

in which ${}^{\circ}G^{am}$ is the Gibbs energy of the system where all the atoms are in the amorphous-like state and its expression is identical with that of solid phase below the melting point except that the term representing the contribution from the high-order anharmonic lattice vibration (T^5 in Eq. (5)) is excluded [6]. ΔG_d is the Gibbs energy difference between liquid-like and amorphous-like states, $\Delta G_d = {}^{\circ}G^{liq} - {}^{\circ}G^{am}$, which can be expressed as:

$$\Delta G_d = A + BT + CT \ln T \tag{9}$$

in which the absolute value of B is recommended as the communal entropy (corresponding to the entropy difference between the atoms in the liquid-like and amorphous-like states), i.e., the gas constant R [6]. The value of B is set equal to -R in the present work. The parameters A and C are optimized based on the experimental information. The experimental enthalpy of fusion is set as the initial value for A. All parameters in Eqs. (8) and (9) are optimized based on the experimental data including the heat capacity, enthalpy, entropy and the melting point.

3.2.2. Solution phases in binary system

In the Ti–V binary system, the Gibbs energies of the solution phases, i.e. liquid, bcc, hcp and ω , are described by the substitutional solution model with the Redlich-Kister polynomial [231]. The molar Gibbs

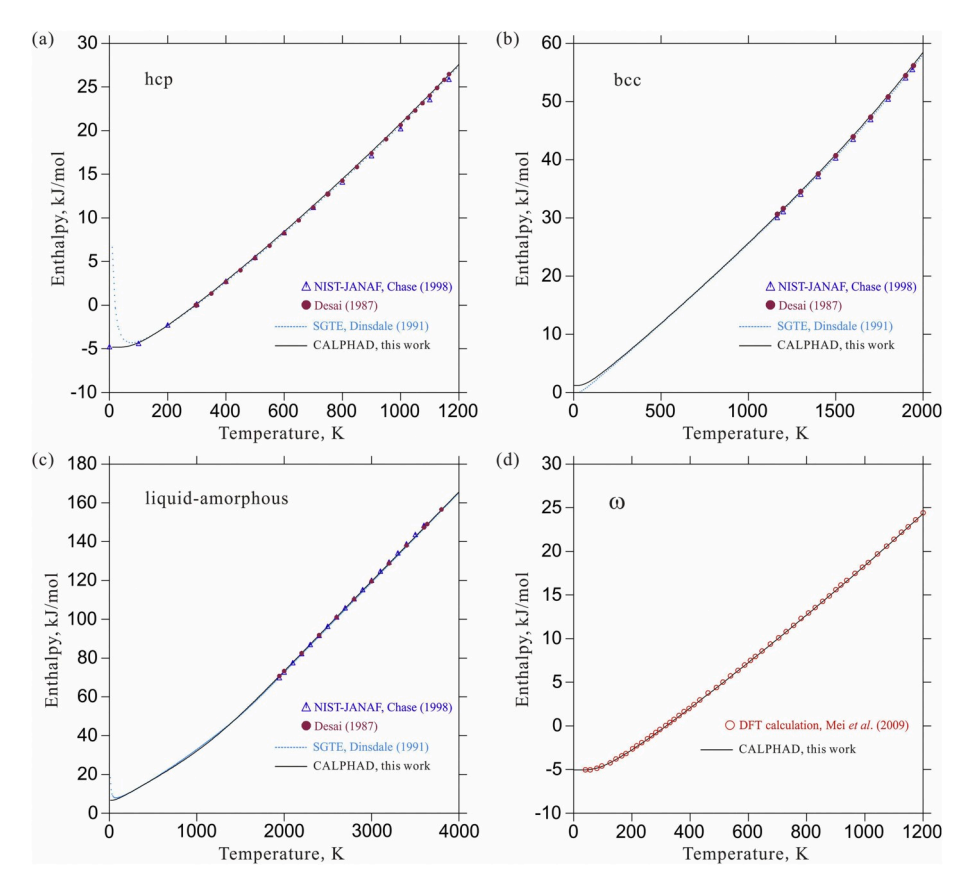


Fig. 6. Calculated enthalpies of (a) hcp, (b) bcc, (c) liquid-amorphous and (d) ω titanium in comparison with literature data and SGTE database [1].

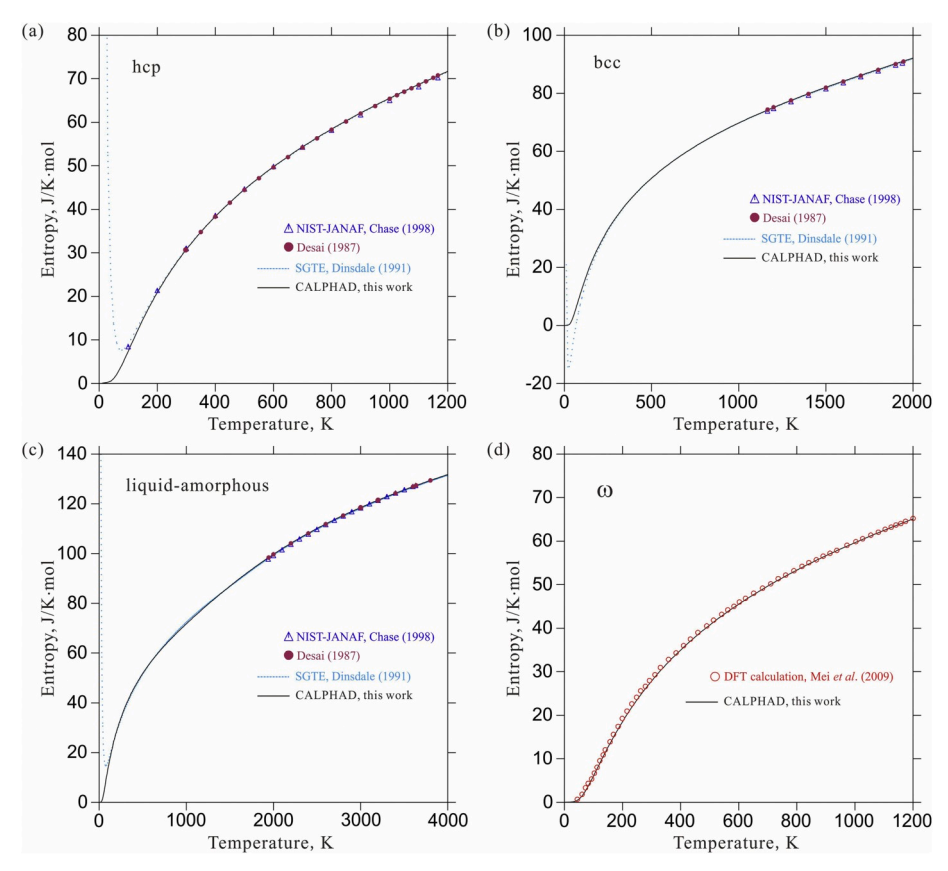


Fig. 7. Calculated entropies of (a) hcp, (b) bcc, (c) liquid-amorphous and (d) ω titanium in comparison with literature data and SGTE database [1].

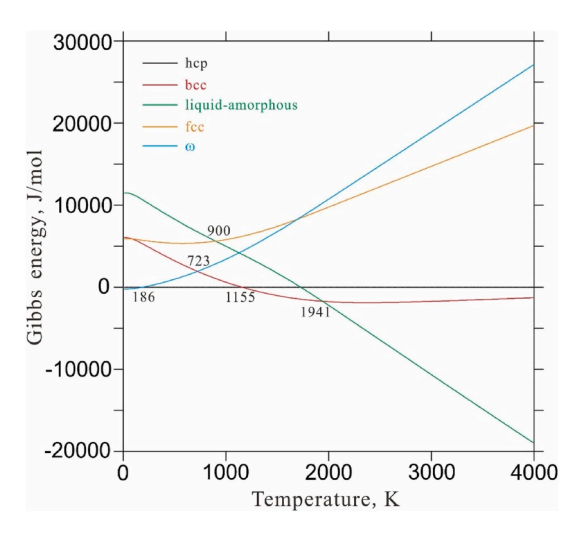


Fig. 8. Calculated Gibbs energies of different allotropes of titanium relative to hcp titanium.

energy of the solution phase ϕ (liquid, bcc, hcp or ω) can be expressed as:

$$G_{m}^{\varphi} - H^{\text{SER}} = x_{\text{Ti}} \cdot {}^{\circ}G_{\text{Ti}}^{\varphi} + x_{\text{V}} \cdot {}^{\circ}G_{\text{V}}^{\varphi} + R \cdot T \cdot (x_{\text{Ti}} \cdot \ln x_{\text{Ti}} + x_{\text{V}} \cdot \ln x_{\text{V}})$$

$$+ x_{\text{Ti}} \cdot x_{\text{V}} \cdot \left[(a_{0} + b_{0} \cdot T) + (a_{1} + b_{1} \cdot T)(x_{\text{Ti}} - x_{\text{V}})^{1} + \dots \right]$$
(10)

in which $H^{\rm SER}$ denotes $x_{\rm Ti} \cdot H^{\rm SER}_{\rm Ti} + x_{\rm V} \cdot H^{\rm SER}_{\rm V}$, and $x_{\rm Ti}$ and $x_{\rm V}$ are the mole fractions of Ti and V, respectively. SER refers to the standard element reference which is the reference state used for each phase in all the CALPHAD-type assessments. The coefficients a_j and b_j (j=0,1...) are the parameters to be optimized with the experimental data as input.

3.2.3. Optimization procedure

Based on the experimental data and theoretical calculations available in the literature and the present work, the Gibbs energy model parameters for Ti, V and the Ti–V system were optimized using the PARROT module [232], which works by minimizing the square sum of the differences between measured and calculated values. During the optimization, each experimental data point was given a certain weight based on uncertainties of the data.

The thermodynamic parameters for the stable phases hcp, bcc and liquid-amorphous titanium, and bcc and liquid-amorphous vanadium were optimized initially. Further, the metastable phases such as fcc and ω titanium/vanadium were optimized. The parameter θ_E in Eqs. (4) and

(5) was optimized based on the experimental heat capacity with the Einstein temperature calculated through the Debye temperature as the starting value. The values of E_0 in Eq. (5) for hcp-Ti and bcc-V were optimized by considering the room temperature enthalpy as reference, i. e., by setting $H^0(298.15 \text{ K})$ to zero. For the other phases, their E_0 values are evaluated based on the calculated ground state energy differences relative to the reference states hcp-Ti and bcc-V by ab initio calculations. The parameter a in Eqs. (4) and (5), which consists of electronic excitations and low-order anharmonic vibrational contributions, was optimized to reproduce experimental heat capacity with the electronic specific heat coefficient for the corresponding phase as initial value. There is no experimental information about the parameter b in Eqs. (4) and (5), which was optimized to fit the heat capacity values. In summary, the parameters E_0 , θ_E , a and b were used to optimize the data including ground state energy differences, Einstein temperature, and experimental heat capacity and enthalpy from 0 K up to the melting point. In order to maintain the continuity in both the heat capacity and its first derivative at the melting temperature, the parameters a', b', and c' in Eqs. (6) and (7) were optimized by setting the heat capacity and its first derivative calculated by Eqs. (4) and (6) equal at the melting point and by requiring that the heat capacity of the solid phase should equal the value of the liquid-amorphous phase at an arbitrarily high temperature much beyond the melting point. The high temperature 4000 K was selected in the present work. The thermodynamic parameters H' and S'in Eq. (7) were optimized on the basis of the enthalpy and entropy at the melting point, respectively. The absolute value of B in Eq. (9) should not be too much different from that of the communal entropy, i.e., the gas constant R [3,230]. In the present optimization, the value of B was fixed to be $-8.314 \text{ J/(mol \cdot K)}$. The parameters A and C in Eq. (9) were optimized based on the experimental heat capacity for the liquid phase, and enthalpy and entropy of fusion. More details about how to optimize parameters in the new thermodynamic model for the third generation thermodynamic databases can be found elsewhere [18].

Based on the Gibbs energy functions for titanium and vanadium obtained in the present work, the thermodynamic reassessment of the Ti–V system was carried out. The liquid, (β Ti, V) and (α Ti) phases in the Ti–V system were treated as subregular solutions, whereas the (ω Ti) phase was modeled as a regular solution.

4. Results and discussion

4.1. Ab initio calculations

The total energy as function of volume for the different allotropes of

Table 13
Summary of the Gibbs energy expressions for vanadium.

Phase	Gibbs energy expressions, J/mol	Temperature range, K
Всс	$GVVBCCL = -8012.67406 - 1.95296216E - 03T^2 - 3.02272704E - 14T^5$	0–2202
	$GVVBCCH = -36942.5742 + 173.1051476T - 21.4019136T \ln(T) \\ -3.45690255E + 19T^{-5} + 7.5656371TE + 38T^{-11}$	2202–6000
	THETA(BCCVV) = LN(265.09)	0–6000
Нер	$GVVHCPL = -4237.42900 - 1.44727302E - 03T^2 - 3.52503774E - 14T^5$	0-2202
	$ \begin{aligned} \text{GVVHCPH} &= -34633.4970 + 174.8234249T - 21.4100569T \ln(T) \\ -3.35922789 \text{E} + 19T^{-5} + 7.18817987 \text{E} + 38T^{-11} \end{aligned} $	2202–6000
	THETA(HCPVV) = LN(283.11)	0–6000
Fcc	$GVVFCCL = -512.674044 - 1.18125097E - 03T^2 - 3.77342177E - 14T^5$	0-2202
	$GVVFCCH = -31683.8285 + 175.6948765T - 21.4090475T \ln(T)$ $-3.35723154E + 19T^{-5} + 7.18557415E + 38T^{-11}$	2202–6000
	THETA(FCCVV) = LN(266.97)	0–6000
Ω	$GVVOMEL = -801.827408 - 1.09936065E - 03T^2 - 3.81357737E - 14T^5$	0-2202
	$ \begin{aligned} \text{GVVOMEH} &= -32200.8701 + 175.8889109T - 21.3974779T \ln(T) \\ -3.50362716E + 19T^{-5} + 7.72223051E + 38T^{-11} \end{aligned} $	2202–6000
	THETA(OMEVV) = LN(247.98)	0–6000
liquid-amorphous	$GVVLIQ = +8708.02961 - 1.87699140E - 03T^2$	0–6000
	THETA(LIQVV) = LN(202.79)	0–6000
	$GD(LIQVV) = +55393.8187 - 8.314T - 0.642018852T \ln(T)$	0–6000

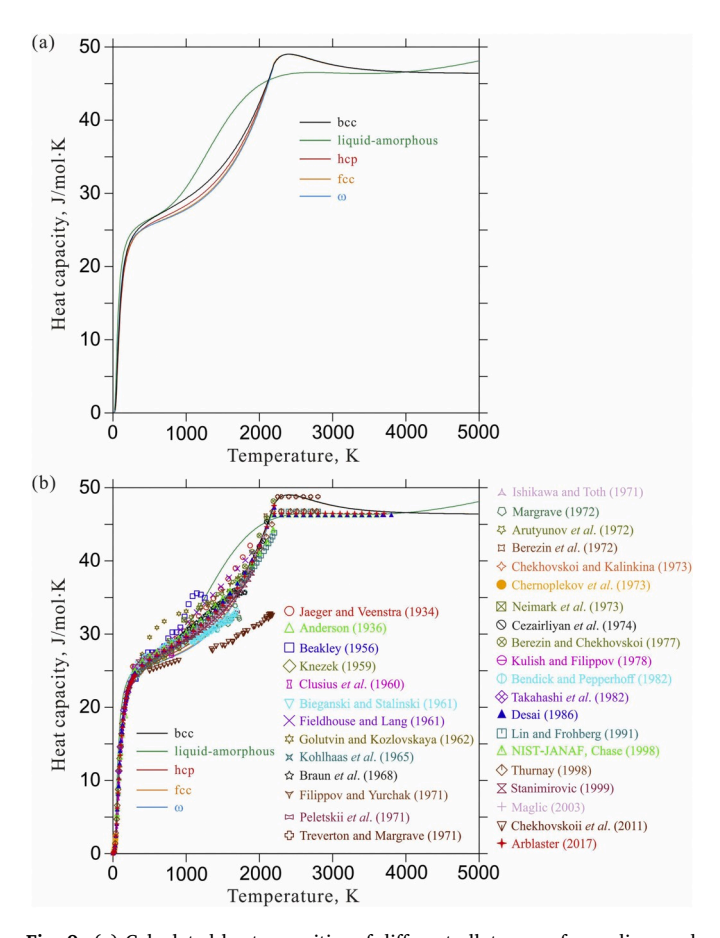


Fig. 9. (a) Calculated heat capacities of different allotropes of vanadium and (b) comparison between the calculated and experimental heat capacities of vanadium.

Ti and V obtained using DFT calculations are shown in Fig. 1. It can be observed from these figures that the stable allotropes for Ti and V at 0 K are ω-Ti and bcc-V, respectively. The results obtained from the DFT calculations for different allotropes of Ti and V are summarized in Table 9, in which the enthalpy differences were computed with respect to the reference state recommended by SGTE (hcp-Ti and bcc-V for Ti and V, respectively). From Fig. 1 and Table 9, it is evident that the order of stability at 0 K for different structures of Ti was $\omega \to hcp \to fcc \to bcc$. Similarly, the order of stability for different structures of V at 0 K is deduced to be $bcc \rightarrow \omega \rightarrow fcc \rightarrow hcp$. The most stable polymorph at 0 K and 0 GPa for Ti was found to be ω-Ti, in contrast to the general behavior where the stable polymorph at room temperature will also be stable at 0 K. This observation is consistent with the results obtained by Argaman et al. [75]. In the case of V, the stable polymorph at room temperature and 0 K are the same, i.e., the bcc-V phase. It is also clear from Table 9 that the initial and calculated lattice parameters for all allotropes of Ti and V are in good agreement with each other. The ΔE values estimated using the DFT calculations for different allotropes are substituted as the initial values of E_0 in Eq. (5).

The independent elastic constants, elastic properties and Debye temperature computed using the ElaStic code for the various allotropes of Ti and V are summarized in Tables 10 and 11. Five and three independent elastic constants are evaluated for the hexagonal and cubic structures, respectively, depending on the symmetry. The stability of a crystal with a particular structure is determined using the Born elastic stability criterion [233]. According to this criterion, a set of conditions involving the independent elastic constants has to be satisfied for a crystal to be dynamically stable. The conditions of stability for a cubic crystal are $C_{11} - C_{12} > 0$, $C_{11} + 2C_{12} > 0$ and $C_{44} > 0$. Similarly, the

conditions required to be satisfied for a hexagonal crystal to be stable are given as $C_{11} > |C_{12}|$, $2C_{13}^2 < C_{33}$, $C_{44} > 0$ and $\frac{(C_{11} - C_{12})}{2} > 0$. It can be clearly observed from Table 10 that the Born elastic stability criterion has not been satisfied for bcc-Ti, fcc-V and hcp-V. This proves that these structures are dynamically unstable at 0 K. Hence, some of the elastic constants calculated for these structures are negative. As a consequence of the dynamic instability possessed by these allotropes, the Debye temperature is calculated to be a complex number with an imaginary part. The calculated Debye temperatures for the stable allotropes of Ti and V are used to compute θ_E in Eqs. (4) and (5).

4.2. Thermodynamic modeling

4.2.1. Lattice stabilities of titanium

The optimized thermodynamic parameters for titanium in the present wok are listed in Table 12. According to the thermodynamic parameters obtained in the present work, the thermodynamic properties of titanium are calculated. The optimized $\theta_{\rm E}$ and a in Eq. (4) for titanium are compared with other values available in the literature in Table 2. The optimized parameters θ_E for hcp, bcc, fcc, ω and liquid-amorphous titanium with the experimental heat capacity as input are in good agreement with the reported Einstein temperatures in the literature. The parameter a for hcp titanium was found to be 7.77, which is larger than the electronic specific heat coefficient (3.332 \pm 0.02 mJ/(mol·K)) recommended by Desai [35]. If the parameter a is kept close to the electronic specific heat coefficient during optimization, the experimental heat capacity cannot be fitted. Furthermore, in the Einstein model, the parameter a includes not only electronic excitations but also low-order anharmonic vibrational contributions. Therefore, the electronic specific heat coefficient is only for reference during the parameter optimization but keeping the parameter a and the electronic specific heat coefficient in the same order of magnitude.

Fig. 2 (a) presents the calculated heat capacities of hcp, bcc, fcc, ω and liquid-amorphous titanium as function of temperature. Fig. 2 (b) shows the comparison between the calculated and experimental heat capacity for different phases. It can be seen that most of the reliable experimental data are reproduced well in the present modeling. The heat capacities of the solid phases approach smoothly to a constant value above the melting point.

The calculated heat capacity of hcp titanium along with the experimental data at 0-300 K and 0-1200 K are shown in Fig. 3(a) and (b), respectively. The agreement is good over the entire temperature range except between 0 and 300 K. The experimental data at between 20 and 70 K are not reproduced in the present modeling since the Einstein model is known to be inadequate [77,84]. The calculated heat capacity between 100 and 300 K is higher by 0.6 J/(mol·K) than the experimental data. It is found that the parameter θ_E is sensitive to the heat capacity at this temperature range during optimization. When the parameter $\theta_{\rm E}$ of hcp titanium is above 290 K, the experimental heat capacity of hcp titanium between 100 and 300 K can be reproduced very well. However, this value is higher by about 20 K than the reported Einstein temperatures [35,78,84,85] listed in Table 2. Hence, the value of $\theta_{\rm E}$ for hcp titanium is given a higher weight than the experimental heat capacity in the temperature range of 100-300 K during the parameter optimization. In comparison with the calculated heat capacity at low temperature from the SGTE database [1], the calculated results from present work are in better agreement with the experimental data.

Fig. 4 (a) is the calculated heat capacity of bcc titanium along with the experimental data and the one from SGTE database [1]. It can be seen that it is in good agreement with the recommend values from Desai [35]. Fig. 4 (b) shows the calculated heat capacity of liquid-amorphous titanium in comparison with experimental data [66–72], recommended data [35,46] and calculated values from SGTE database [1]. Both the measured and recommended heat capacities of the liquid-amorphous phase are a constant. In the present work, the liquid and amorphous

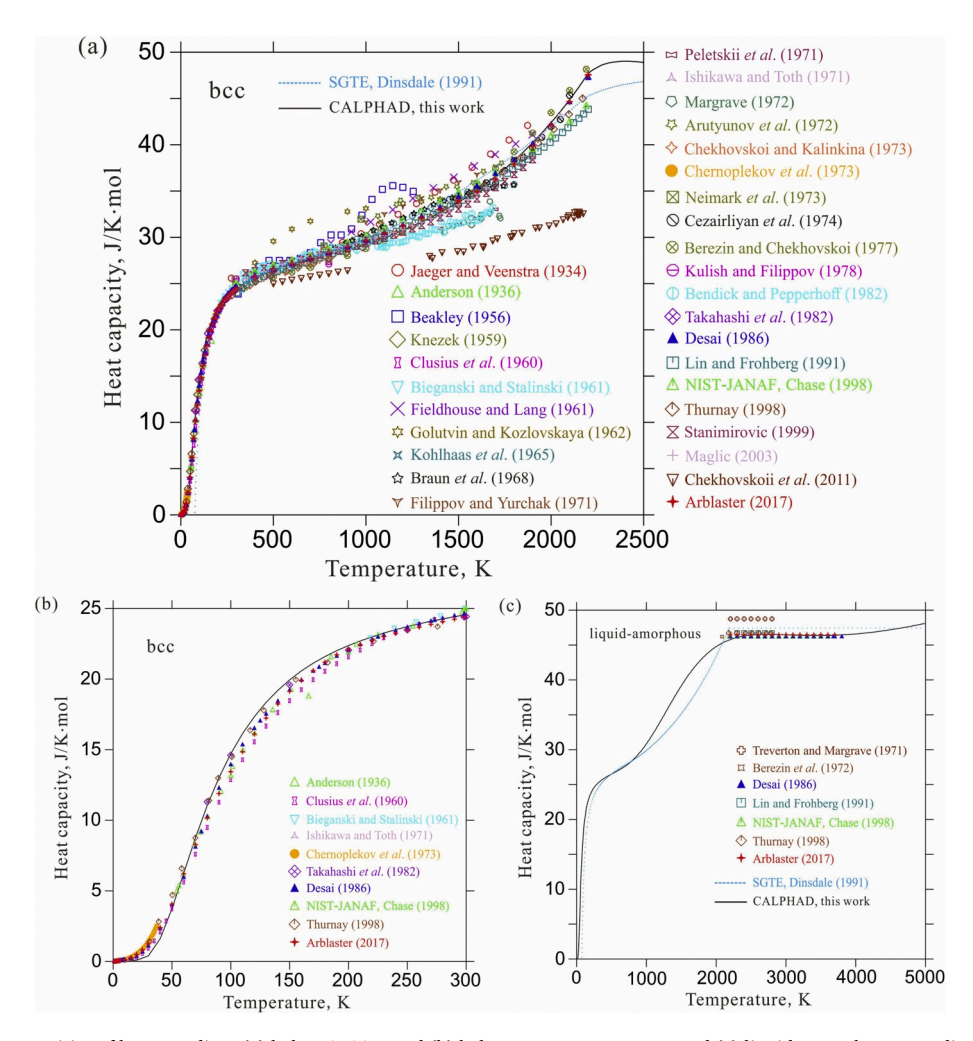


Fig. 10. Calculated heat capacities of bcc vanadium (a) below 2500 K and (b) below room temperature, and (c) liquid-amorphous vanadium in comparison with the experimental data and SGTE database [1].

phases of titanium have been described as one phase by a generalized two-state model, which is ideal for the description of the temperature dependence of heat capacity experimentally found for substances with a strong tendency to form amorphous structure. If one allows the parameter B in Eq. (9) to vary during the optimization, the calculated heat capacity of the liquid-amorphous phase above the melting point approaches a constant value, but then, the value of B will be very different from that of the communal entropy. Therefore, the value of *B* is fixed to be -8.314 with more physical meaning and the calculated heat capacity of liquid-amorphous titanium is probably closer to reality. The calculated heat capacity from the present work for liquid-amorphous titanium is well within the experimental uncertainties 46.29 \pm 1.7 J/(mol·K) [35]. Fig. 4 (c) presents the calculated heat capacity of fcc titanium along with the calculated data using ab initio calculations from Zhang et al. [73] and SGTE database [1]. As can be seen from Fig. 4 (c), the calculated heat capacity of fcc titanium in the present work is higher than the value from DFT calculations. In comparison with the heat capacities of other solid phase, the slope of calculated heat capacity of fcc titanium by DFT calculations [73] is lower. Therefore, the data calculated by DFT calculations from Zhang et al. [73] are questionable and the calculated heat capacity from present work for fcc titanium is acceptable. Fig. 4 (d) is the calculated heat capacity of ω phase in comparison with the data calculated by DFT calculations from Mei et al. [74] and Argaman et al. [75]. It can be seen that the agreement is very good.

Fig. 5(a) and (b) are the calculated increments of enthalpy $H_m(T)-H_m(298.15\ K)$ and entropy $S_m(T)-S_m(298.15\ K)$ of titanium compared

with experimental data [67,68,106], recommended values [35] and SGTE database [1]. The experimental and recommended data are reproduced well in the present optimization. The calculated transition enthalpy and entropy between hcp and bcc, and enthalpy and entropy of fusion for titanium are compared with experimental and assessed values in Table 3. It is evident that the calculated values are in good agreement with the experimental and recommended values.

Fig. 6(a) to (d) and Fig. 7(a) to (d) present the calculated enthalpies and entropies of hcp, bcc, liquid-amorphous and ω titanium, respectively, in comparison with the recommended values from NIST-JANAF [46] and Desai [35], DFT calculations [74] and SGTE database [1]. From these figures, it can be seen that the agreement is very good. We also see clearly that the second generation thermodynamic models [1] cannot reproduce the enthalpy and entropy of pure titanium at low temperature. The third generation thermodynamic models with definite physical meaning can describe accurately the enthalpy and entropy from high temperature down to 0 K.

The calculated Gibbs energies of bcc, liquid-amorphous, fcc and ω titanium relative to hcp titanium are shown in Fig. 8. The intersections of the lines for the bcc phase with the hcp and liquid-amorphous phases are at 1155 and 1941 K, respectively. It means that the calculated transition temperature between hcp and bcc is 1155 K and the melting point of titanium is 1941 K, which are equal to the widely accepted values [1]. The calculated transition temperatures of $T_{\omega\text{-hcp}}$ and $T_{\omega\text{-bcc}}$ are found to be 186 and 723 K, respectively. These values are equal to the values given by Mei et al. [74] and Mirzayev et al. [112], respectively. The transition temperature of $T_{\text{fcc-liquid}}$ is calculated to be 900 K,

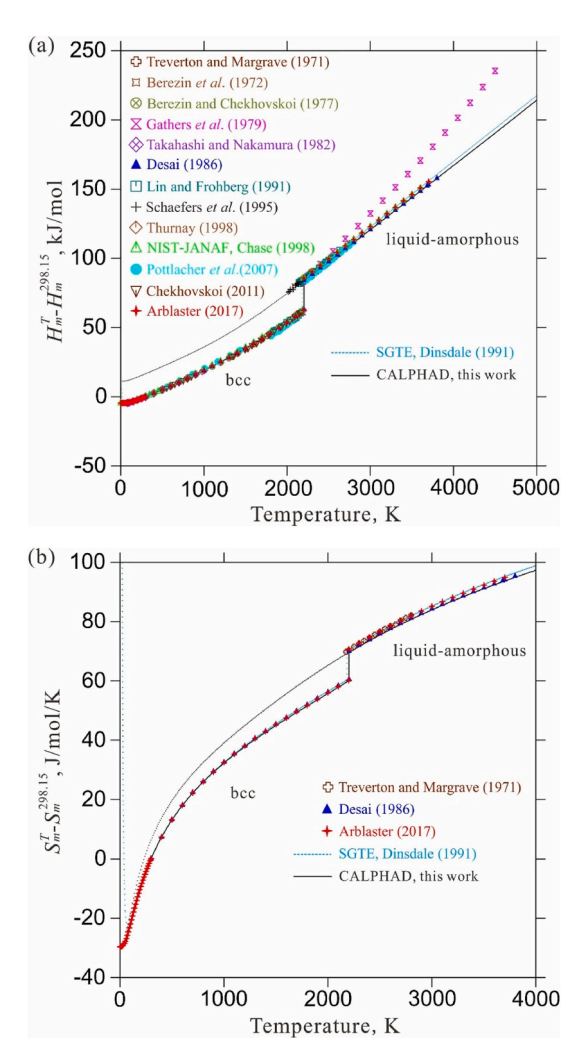


Fig. 11. Calculated the increments of (a) enthalpy $H_m(T) - H_m(298.15 \ K)$ and (b) entropy $S_m(T) - S_m(298.15 \ K)$ of vanadium in comparison with experimental data, recommended values and SGTE database [1].

which is consistent with the value from the SGTE database [1].

The calculated ground state energy differences ΔE for bcc, fcc and ω relative to hcp titanium at 0 K by ab initio calculations and CALPHAD approach are listed in Table 4. As can be seen from this table, the values calculated by ab initio calculations in the present work are consistent with the corresponding values from the literature [74,75,89,109,111]. The calculated $\Delta E_{\text{fcc-hcp}}$ and $\Delta E_{\omega\text{-hcp}}$ by the CALPHAD approach in the present work are in good agreement with the ones by ab initio calculations, while the CALPHAD calculated result of $\Delta E_{\text{bcc-hcp}}$ is much lower than the value from ab initio calculations. By a systematic comparison of bcc-fcc and bcc-hcp phase stabilities from ab initio calculations [109] and the SGTE database [1], Yan and Olson [88] proposed a factor of 0.357 to convert ab initio calculated phase stabilities to the values that can be adopted in the CALPHAD approach when the ab initio calculated values are large. In the present work, the ab initio calculations are given a low weight when they are large during the parameter optimization. Combining Figs. 8 and 1, both of the results obtained by the CALPHAD method and ab initio calculations show that the order of stability of different allotropes for titanium at 0 K is $\omega \to hcp \to fcc \to bcc$, which is consistent with the literature data [1,74,75,89,109–111].

4.2.2. Lattice stabilities of vanadium

The optimized thermodynamic parameters for vanadium in the present wok are listed in Table 13. The thermodynamic properties of vanadium are calculated according to the thermodynamic parameters

obtained in the present work. The optimized parameters $\theta_{\rm F}$ and a in Eq. (4) for vanadium in comparison with literature data are listed in Table 6. The θ_E value for bcc vanadium was optimized to be 265.09 K, which is in good agreement with the recommended values 258.40 K [115] and 266.59 K [116], and the ones from DFT calculations 256.33 K [85] and 265.78 K (the present work). The calculated $\theta_{\rm E}$ values of hcp and bcc vanadium are consistent with the values from Li et al. [167]. For the ω vanadium, the optimized $\theta_{\rm E}$ value (247.98 K) is larger than the computed value from ab initio calculations (230.88 K) in the present work. If the *ab initio* calculated θ_E is adopted, the calculated ground state energy difference between ω and bcc will decrease with the increase of the temperature. It indicates that the ω phase is stable at high temperature, which is not reasonable. In order to circumvent this problem, a larger θ_E of ω vanadium is recommended. For the liquid-amorphous phase, the optimized θ_E value of 202.79 K is in good agreement with the predicted value 201 \pm 19 K according to the assumption from Grimvall [96]. The optimized parameter a of bcc, hcp, fcc, ω and liquid-amorphous vanadium are smaller than the corresponding electronic specific heat coefficient from Desai [115], Arblaster [116] and Li et al. [167]. If the electronic specific heat coefficient is given a large weight during the optimization of parameter a, the experimental heat capacity cannot be fitted well. Similarly, the electronic specific heat coefficient of vanadium is only for reference in the parameter optimization but the parameter a and the electronic specific heat coefficient should be kept in the same order of magnitude.

Fig. 9 (a) shows the calculated heat capacities of bcc, hcp, fcc, ω and liquid-amorphous vanadium as a function of temperature according to the present thermodynamic modeling. Fig. 9 (b) is the comparison between the calculated and experimental heat capacity. Most of the reliable experimental data are reproduced well in the present work. The calculated heat capacities of the metastable phases hcp, fcc and ω vanadium are almost equal to the heat capacity of bcc vanadium above melting point. The calculated heat capacities for all solid phases, as can be seen in Fig. 9, approach smoothly a constant value above the melting point.

The calculated heat capacity of bcc vanadium along with the experimental data and the vales from SGTE database [1] in the temperature range of 0-2500 K is shown in Fig. 10 (a). It can be seen that most of the reliable experimental data are fitted well over the entire temperature range. The heat capacity of bcc vanadium between 0 and 300 K is calculated along with the experimental data in Fig. 10 (b). A perfect fitting is not expected in the low temperature region since the Einstein model is inadequate and only one parameter $\theta_{\rm F}$ has been used to represent the phonon density of states. However, an important improvement of the third generation models is the more physical treatment of the low-temperature region compared with the second generation SGTE database [1]. Fig. 10 (c) shows the calculated heat capacity of liquid-amorphous vanadium in comparison with experimental data [67,113,155,156], recommended data [46,115,116] and calculated one from SGTE database [1]. Similar to the liquid-amorphous titanium, the value of parameter B in Eq. (9) for the liquid-amorphous vanadium is fixed to be -8.314 with more physical meaning and the calculated heat capacity of liquid-amorphous vanadium is in good agreement with the recommend values [46,115,116] within the experimental uncertainties.

The calculated increments of enthalpy $H_m(T) - H_m(298.15 \, K)$ and entropy $S_m(T) - S_m(298.15 \, K)$ of vanadium in comparison with literature data and SGTE database [1] are shown in Fig. 11(a) and (b). The experimental data and recommended values are reproduced well by the present calculation except the experimental data from Gathers et al. [168]. As mention above, the values from Gathers et al. [168] are higher than the recommended values [46,115,116] at high temperatures. Thus, the experimental data from Gathers et al. [168] are not used in the present work but only for comparison. The calculated enthalpy and entropy of fusion for vanadium in comparison with experimental data and recommended values are listed in Table 7. It is can be seen that the

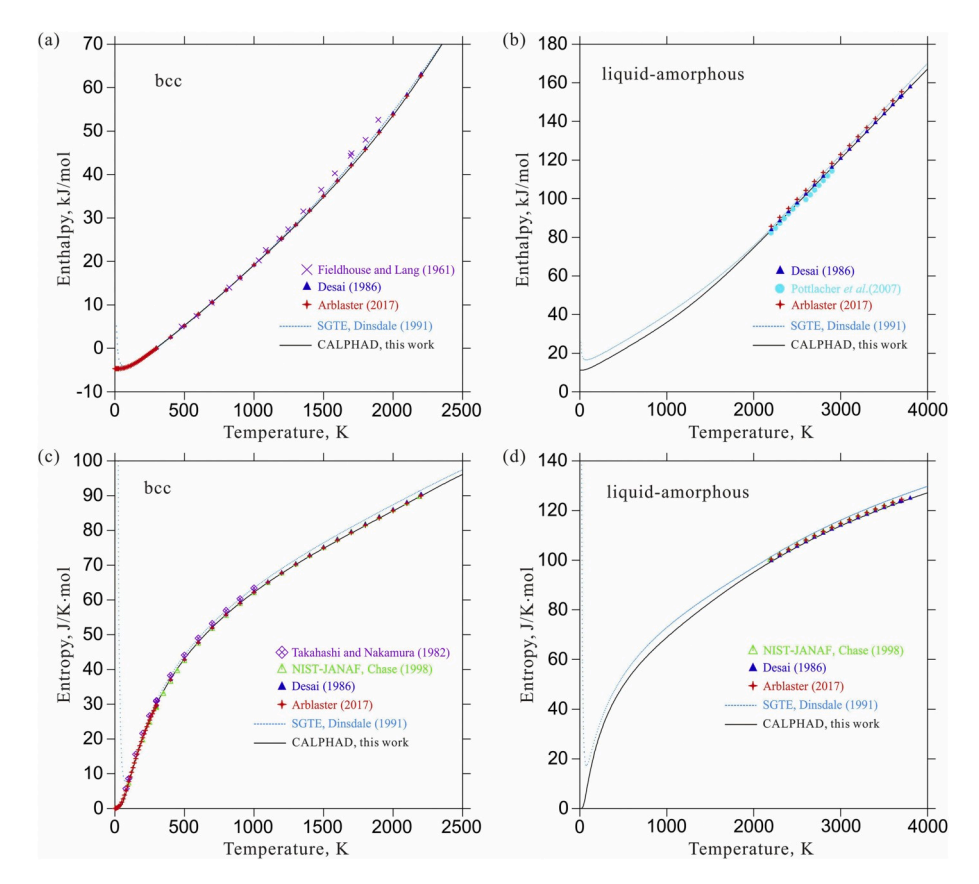


Fig. 12. Calculated enthalpies of (a) bcc and (b) liquid-amorphous, and entropies of (c) bcc and (d) liquid-amorphous for vanadium in comparison with experimental data, recommended values and SGTE database [1].

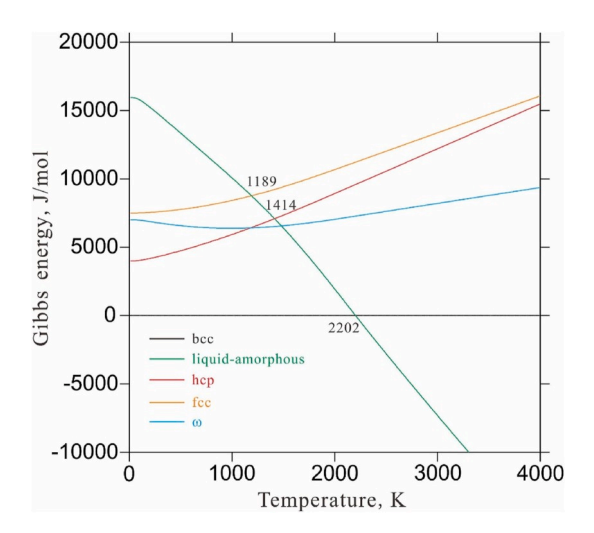


Fig. 13. Calculated Gibbs energies of different allotropes of vanadium relative to bcc vanadium.

calculated values are in good agreement with the experimental data and recommended values.

Fig. 12(a) to (d) present the calculated enthalpies and entropies of bcc and liquid-amorphous vanadium, respectively, in comparison with the experimental data [136,140], recommended values [46,115,116], and SGTE database [1]. From these figures, it is clear that the agreement is much better than the ones from SGTE database at low temperature. Again, the third generation thermodynamic models with definite physical meaning adopted in the present work can describe accurately the enthalpy and entropy of vanadium from 0 K to high temperature.

Table 14Summary of the optimized thermodynamic parameters in the Ti–V system.

Phases	Models	Thermodynamic parameters
Liquid	(Ti, V) ₁	$^{0}L_{\mathrm{Ti,V}}^{\mathrm{Liquid}}=163.57$
		$^{1}L_{ m Ti,V}^{ m Liquid} = 2896.31$
(βTi, V)	$(Ti, V)_1Va_3$	$^{0}L_{\mathrm{Ti,V}}^{(\beta\mathrm{Ti,V})} = 6625.26$
		$^{1}L_{\mathrm{Ti,V}}^{(\beta\mathrm{Ti,V})} = 1676.53$
(αTi)	$(Ti, V)_1 Va_{0.5}$	$^{0}L_{\text{Ti,V:Va}}^{(\alpha\text{Ti})} = 44830.75 - 10T$
		$^{1}L_{\text{Ti,V:Va}}^{(\alpha\text{Ti})} = -26396.30$
(ωTi)	$(Ti, V)_1 Va_{0.5}$	$^{0}L_{\mathrm{Ti,V:Va}}^{(\omega\mathrm{Ti})} = 8000 - 8T$

The calculated Gibbs energies of hcp, fcc, ω and liquid-amorphous vanadium relative to bcc vanadium are shown in Fig. 13. The intersection of the lines between the bcc and liquid-amorphous phases is at 2202 K. It shows that the calculated melting point of vanadium is 2202 K, which is also listed in Table 7 along with the experimental and assessed melting point of vanadium. In comparison with the melting point (1983 K) of vanadium in the second generation thermodynamic database [1], it is updated in the present work according to the recommended values 2202 K and 2201 \pm 6 K from Desai [115] and Arblaster [116], respectively. The intersections of the lines for the liquid-amorphous phase with the hcp and fcc phases are 1414 and 1189 K, respectively, where hcp and fcc vanadium would melt metastably. These calculated melting points for metastable hcp and fcc vanadium are consistent with the values from the SGTE database [1].

The calculated ground state energy differences ΔE for hcp, fcc and ω relative to bcc vanadium at 0 K by *ab initio* calculations and CALPHAD approach are listed in Table 8. It can be seen that the values calculated

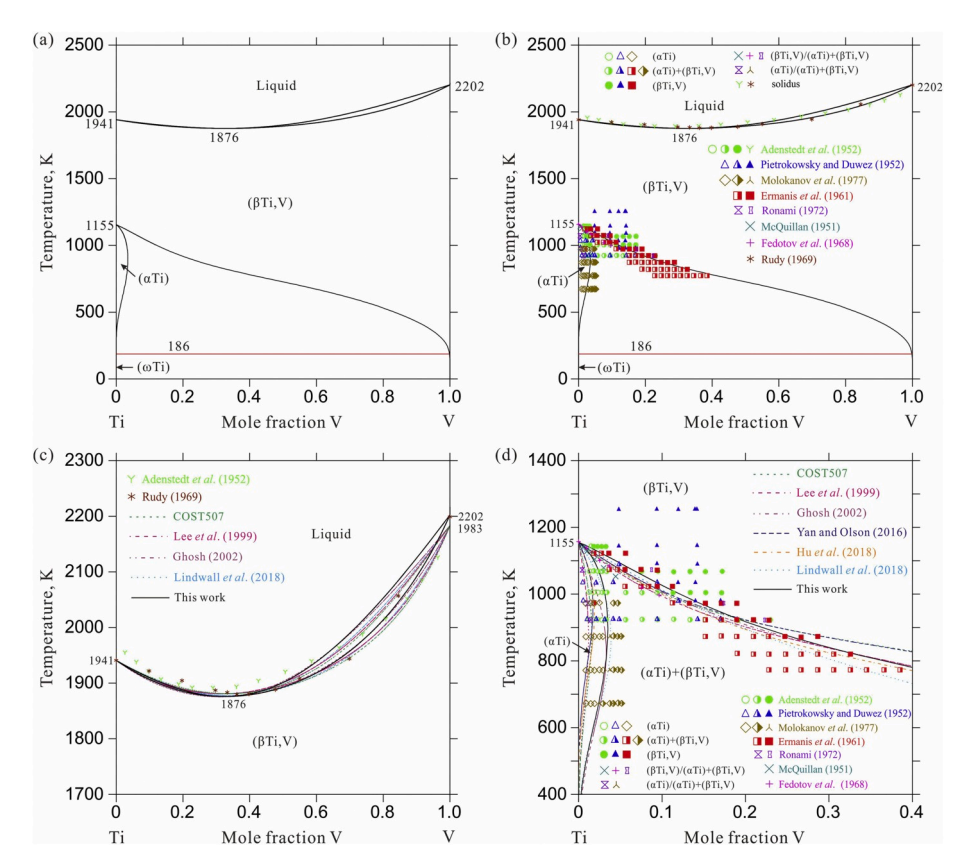


Fig. 14. (a) Calculated phase diagram of the Ti–V system, (b) comparison between the calculated phase diagram and experimental data, (c) enlargement of liquidus and solidus and (d) enlargement of solid phase boundaries in Ti–rich side.

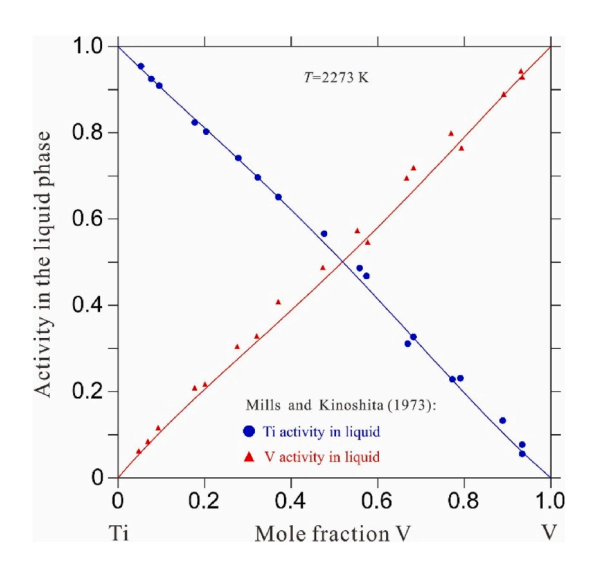


Fig. 15. Calculated activities of V and Ti in the liquid phase at 2273 K in comparison with experimental data [191].

by *ab initio* calculations in the present work are consistent with the corresponding ones from the literature [88,109,111]. However, as discussed above, if the values of ground state energy differences ΔE calculated by *ab initio* calculations are large relative to the ones suggested by the SGTE database, they may not be directly applicable to a CALPHAD assessment. Here, the values from *ab initio* calculations are given a low weight in the present work. Since only few experimental data are available for metastable hcp and fcc vanadium, their ground state energy differences relative to bcc vanadium were calculated from the SGTE database [1] and adopted in the present optimization.

Combining with Fig. 13 and Table 8, the calculated order of stability of different solid phases for vanadium at 0 K is $bcc \rightarrow hcp \rightarrow \omega \rightarrow fcc$ by the CALPHAD approach, which is consistent with the SGTE database [1].

4.3. The Ti-V system

The optimized thermodynamic parameters for the Ti-V system in the present wok are summarized in Table 14. The calculated phase diagram of the Ti-V system by the present modeling is shown in Fig. 14 (a). In the present modeling, the (ωTi) phase is included and it forms from the peritectoid reaction (αTi) + (βTi , V) \rightarrow (ωTi) at 186 K. Fig. 14 (b) is the comparison between the calculated phase diagram and experimental data [183-189,210]. Fig. 14(c) and (d) shows the enlargements of the Ti-V phase diagram above 1700 K and below 1400 K, respectively, compared with the experimental data and previous thermodynamic assessments [88,175–178,217]. As can be seen from these figures, most of the reliable experimental data are reproduced well by the obtained thermodynamic parameters in the present work. In Fig. 14 (c), the calculated congruent minimum between liquidus and solidus is at 33 at. % V and 1876 K, which is consistent with the reported values (35 at.% V and 1877 \pm 5 K) [184]. Since the experimental points of solidus from Adenstedt et al. [183] and Rudy [184] are scattered, only part of experimental data are reproduced in the present work and the calculated liquidus and solidus from the present work are similar to the previously calculated ones [175-178]. Specifically, the calculated liquidus and solidus almost overlap the widely accepted ones from Ghosh [177] except for the V-rich side. This is because the melting point of vanadium is updated from 1983 to 2202 K. In Fig. 14 (d), the calculated phase boundaries $(\alpha Ti)/(\alpha Ti)+(\beta Ti, V)$ and $(\beta Ti, V)/(\alpha Ti)+(\beta Ti, V)$ are in good agreement with the experimental data [183,185-189,210]. Compared with the previously calculated phase boundaries [88,175–178,217], the calculated ones from the present work are consistent with the widely

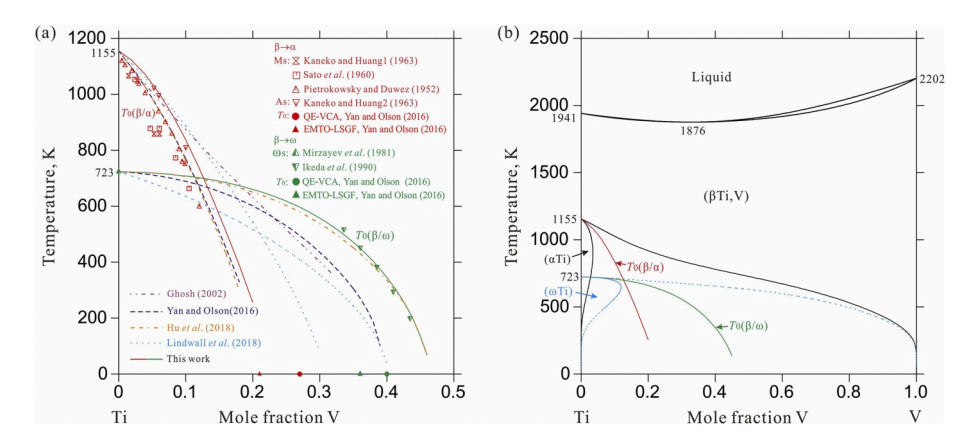


Fig. 16. (a) Calculated $T_0(\beta/\alpha)$ and $T_0(\beta/\alpha)$ curves in comparison with the experimental data and the ones from other works [88,178,217], and (b) calculated metastable phase diagram of the Ti–V system with $T_0(\beta/\alpha)$ and $T_0(\beta/\alpha)$ curves.

accepted ones from Ghosh [177]. In addition, the calculated phase regions of (α Ti) from COST507 [175], Lee et al. [176], Yan and Olson [88] and Hu et al. [217] are much smaller than the experimental data.

Fig. 15 presents the calculated activities of vanadium and titanium in the liquid phase at 2273 K in comparison with experimental data [191]. It can be seen that the reasonable agreement is obtained.

The calculated $T_0(\beta/\alpha)$ and $T_0(\beta/\omega)$ curves of the Ti–V system along with the experimental data [202,206,208,210,212,213], ab initio calculations [88] and the ones from Ghosh [177], Yan and Olson [88], Hu et al. [217] and Lindwall et al. [178] are shown in Fig. 16 (a). The thermodynamic description for the equilibrium α , the hcp α' martensite and the orthorhombic $\alpha^{\prime\prime}$ martensite is unified in the current treatment due to the continuity of M_s temperature at α' and α'' transition composition. For the $T_0(\beta/\alpha)$ curve, the present calculated results agree better than the ones from Ghosh [177] and Lindwall et al. [178] with the experimental data. Although the calculated $T_0(\beta/\alpha)$ curve from Yan and Olson [88], and Hu et al. [217] are also in good agreement with experimental data, the calculated phase regions for hcp from their work are much smaller than the experimental data (as shown in Fig. 14 (d)). The difference of A_s – M_s is small for the Ti–V system, thus the thermoelastic martensitic transformation is assumed. The calculated $T_0(\beta/\alpha)$ is larger than M_s , which is in conformity with actual situation. For the $T_0(\beta/\omega)$ curve, both the calculated results from the present work and Hu et al. [217] are in good agreement with the experimental data [212, 213]. In the present work, the ω_s temperatures reported in the literature are adopted and treated as $T_0(\beta/\omega)$. The calculated $T_0(\beta/\omega)$ curves from Yan and Olson [88] and Lindwall et al. [178] are lower than the experimental data [213] because they just reproduced the values from the ab initio calculations [88] and gave a low weight to the experimental data [213]. Both the $T_0(\beta/\alpha)$ and $T_0(\beta/\omega)$ curves extend downward with the increase of V compositions. The intersection of $T_0(\beta/\alpha)$ and $T_0(\beta/\omega)$ terminates the martensitic transformation at about 700 K. It indicates that the formation of the ω phase is competitive to the martensitic transformation. Fig. 16 (b) shows calculated metastable phase diagram of the Ti–V system in blue dashed lines with $T_0(\beta/\alpha)$ and $T_0(\beta/\omega)$ curves. The metastable phase diagrams of the Ti-V system can be calculated using the parameters from present work by suspending the (α Ti) phase. The calculated results show that the (ωTi) phase has a large solubility of about 12 at.% V.

5. Conclusions

 The thermodynamic properties of titanium and vanadium and phase equilibria of the Ti–V system have been critically reviewed. The Debye temperatures and enthalpy differences at 0 K of different allotropes for titanium and vanadium have been computed by ab initio calculations to supply the necessary thermodynamic data for the modeling.

- A new model considering lattice vibration, electronic excitation, and anharmonic vibration contributions has been used to describe the Gibbs free energy of the crystalline phases for titanium and vanadium. The generalized two-state model has been adopted for the liquid-amorphous phase. The third generation thermodynamic descriptions for titanium and vanadium from high temperature down to 0 K have been developed by the CALPHAD approach. The thermodynamic properties including heat capacity, enthalpy, and entropy are reproduced well by the obtained thermodynamic parameters.
- The Ti–V system has been reassessed based on the new Gibbs energy functions of titanium and vanadium and experimental data available in the literature. The martensitic transformation and metastable ω phase formation have been thermodynamically described. The partitionless equilibrium temperatures T_0 between β and α/ω have been reproduced well compared with the literature data. The metastable phase diagram of the Ti–V system as well as the $T_0(\beta/\alpha)$ and $T_0(\beta/\omega)$ curves are calculated. The calculated results are in good agreement with the experimental data.
- The thermodynamic parameters of the Ti–V system obtained in the present work enrich the third generation thermodynamic databases. This work can provide the important thermodynamic data for the study of the martensitic transformation and metastable ω phase formation in Ti–V based alloys.

Declaration of competing interest

The authors declared that there are no conflicts of interest for this work.

CRediT authorship contribution statement

Biao Hu: Investigation, Methodology, Writing - original draft, Writing - review & editing, Funding acquisition. **Soumya Sridar:** Investigation, Methodology, Writing - original draft, Writing - review & editing. **Liangyan Hao:** Methodology, Writing - review & editing. **Wei Xiong:** Methodology, Supervision, Writing - review & editing, Funding acquisition.

Acknowledgments

B. Hu acknowledges the financial support from Anhui Province University Natural Science Research Projects of China (No. KJ2019A0113), National Natural Science Foundation of China (No. 51501002), China Postdoctoral Science Foundation (No. 2015M581972) and Anhui Province Postdoctoral Science Foundation of

China (No. 2017B210). W. Xiong acknowledges funding from the National Science Foundation under award DMR-1808082, and from the University of Pittsburgh through the Central Research Development Fund (CRDF).

Appendix A. Supplementary data

Supplementary data to this article can be found online at https://doi.org/10.1016/j.intermet.2020.106791.

References

- [1] A.T. Dinsdale, SGTE data for pure elements, Calphad 15 (1991) 317-425.
- [2] M.W. Chase, I. Ansara, A. Dinsdale, G. Eriksson, G. Grimuval, L. Hoglund, H. Yokokawa, Workshop on thermodynamic models and data for pure elements and other endmembers of solutions: group 1: heat capacity models for crystalline phases from 0 K to 6000 K, Calphad 19 (1995) 437–447.
- [3] J. Agren, B. Cheynet, M.T. Clavaguera-Mora, K. Hack, J. Hertz, F. Sommer, U. Kattner, Workshop on thermodynamic models and data for pure elements and other endmembers of solutions: group 2: extrapolation of the heat capacity in liquid and amorphous phases, Calphad 19 (1995) 449–480.
- [4] A. Chang, C. Colinet, M. Hillert, Z. Moser, J.M. Sanchez, N. Saunders, R. E. Watson, A. Kussmaul, Workshop on thermodynamic models and data for pure elements and other endmembers of solutions: Goup 3: estimation of enthalpies for stable and metastable states, Calphad 19 (1995) 481–498.
- [5] D. de Fontaine, S.G. Fries, G. Inden, G. Miodownik, R. Schmid-Fetzer, S.-L. Chen, Workshop on thermodynamic models and data for pure elements and other endmembers of solutions: group 4: Lambda-transitions, Calphad 19 (1995) 499_536
- [6] Q. Chen, B. Sundman, Modeling of thermodynamic properties for bcc, fcc, liquid, and amorphous iron, J. Phase Equil. 22 (2001) 631–644.
- [7] S. Bigdeli, H. Mao, M. Selleby, On the third-generation Calphad databases: an updated description of Mn, Phys. Status Solidi B 252 (2015) 2199–2208.
- [8] S. Bigdeli, H. Ehtehsami, Q. Chen, H. Mao, P. Korzhavy, M. Selleby, New description of metastable hcp phase for unaries Fe and Mn: coupling between first-principles calculations and CALPHAD modeling, Phys. Status Solidi B 253 (2016) 1830–1836.
- [9] Z. Li, S. Bigdeli, H. Mao, Q. Chen, M. Selleby, Thermodynamic evaluation of pure Co for the third generation of thermodynamic databases, Phys. Status Solidi B 254 (2017) 1600231.
- [10] Z. Li, H. Mao, M. Selleby, Thermodynamic modeling of pure Co accounting two magnetic states for the Fcc phase, J. Phase Equilibria Diffus. 39 (2018) 502–509.
- [11] A.V. Khvan, A.T. Dinsdale, I.A. Uspenskaya, M. Zhilin, T. Babkina, A.M. Phiri, A thermodynamic description of data for pure Pb from 0 K using the expanded Einstein model for the solid and the two state model for the liquid phase, Calphad 60 (2018) 144–155.
- [12] S. Bigdeli, Q. Chen, M. Selleby, A new description of pure C in developing the third generation of Calphad databases, J. Phase Equilibria Diffus. 39 (2018) 832–840.
- [13] T. Omori, S. Bigdeli, H. Mao, A generalized approach obeying the third law of thermodynamics for the expression of lattice stability and compound energy: a case study of unary aluminum, J. Phase Equilibria Diffus. 39 (2018) 519–531.
- [14] S. Bigdell, L.F. Zhu, A. Glensk, B. Grabowski, B. Lindahl, T. Hickel, M. Selleby, An insight into using DFT data for Calphad modeling of solid phases in the third generation of Calphad databases, a case study for Al, Calphad 65 (2019) 79–85.
- [15] A.V. Khvan, T. Babkina, A.T. Dinsdale, I.A. Uspenskaya, Î.V. Fartushna, A. I. Druzhinina, A.B. Syzdykova, M.P. Belov, I.A. Abrikosov, Thermodynamic properties of tin: Part I Experimental investigation, ab-initio modelling of α-, β-phase and a thermodynamic description for pure metal in solid and liquid state from 0 K, Calphad 65 (2019) 50–72.
- [16] A.V. Khvan, I.A. Uspenskaya, N.M. Aristova, Q. Chen, G. Trimarchi, N. M. Konstantinova, A.T. Dinsdale, Description of the thermodynamic properties of pure gold in the solid and liquid states from 0 K, Calphad 68 (2020) 101724.
- [17] A. Dinsdale, O. Zobac, A. Kroupa, A. Khvan, Use of third generation data for the elements to model the thermodynamics of binary alloy systems: Part 1-The critical assessment of data for the Al–Zn system, Calphad 68 (2020) 101723.
- [18] L.Y. Hao, W. Xiong, The Third-Generation CALPHAD Database: A Case Study of Cr–Ni, Calphad, 2020 to be submitted.
- [19] W. Xiong, P. Hedström, M. Selleby, J. Odqvist, M. Thuvander, Q. Chen, An improved thermodynamic modeling of the Fe-Cr system down to zero kelvin coupled with key experiments, Calphad 35 (2011) 355–366.
- [20] W. Xiong, Thermodynamic and Kinetic Investigation of the Fe-Cr-Ni System Driven by Engineering Applications, Ph.D. thesis, KTH Royal Institute of Technology, Sweden, 2012.
- [21] G. Lutjering, J.C. Williams, Titanium, Springer, New York, 2007.
- [22] B. Hu, B. Yao, J. Wang, Y. Liu, C.J. Wang, Y. Du, H.Q. Yin, The phase equilibria of the Ti–V–M (M = Si, Nb, Ta) ternary systems, Intermetallics 118 (2020) 106701.
- [23] B. Hu, C.L. Qiu, S.L. Cui, P.S. Wang, J.Q. Zhou, W.S. Xu, F.F. Min, J.R. Zhao, CALPHAD-type thermodynamic description of phase equilibria in the Ti–W–M (M = Zr, Mo, Nb) ternary systems, J. Chem. Thermodyn. 131 (2019) 25–32.

- [24] B. Hu, J.Q. Zhou, Y.T. Meng, P.S. Wang, C.L. Qiu, F.F. Min, J.R. Zhao, CALPHADtype thermodynamic modeling of the Ti–W–B and Ti–W–Si refractory systems, Int. J. Refract. Metals Hard Mater. 81 (2019) 206–213.
- [25] Y. Ohmori, T. Ogo, K. Nakai, S. Kobayashi, Effects of ω -phase precipitation on $\beta \to \alpha$, α'' transformations in a metastable β titanium alloy, Mater. Sci. Eng., A 312 (2001) 182–188.
- [26] F. Prima, P. Vermaut, G. Texier, D. Ansel, T. Gloriant, Evidence of α-nanophase heterogeneous nucleation from ω particles in a β-metastable Ti-based alloy by high-resolution electron microscopy, Scripta Mater. 54 (2006) 645–648.
- [27] S. Nag, R. Banerjee, R. Srinivasan, J.Y. Hwang, M. Harper, H.L. Fraser, ω-Assisted nucleation and growth of α precipitates in the Ti–5Al–5Mo–5V–3Cr–0.5Fe β titanium alloy, Acta Mater. 57 (2009) 2136–2147.
- [28] T. Li, D. Kent, G. Sha, M.S. Dargusch, J.M. Cairney, The mechanism of ω -assisted α phase formation in near β -Ti alloys, Scripta Mater. 104 (2015) 75–78.
- [29] Y. Zheng, D. Choudhuri, T. Alam, R.E.A. Williams, R. Banerjee, H.L. Fraser, The role of cuboidal ω precipitates on α precipitation in a Ti–20V alloy, Scripta Mater. 123 (2016) 81–85.
- [30] Y. Zheng, R.E.A. Williams, D. Wang, R.P. Shi, S. Nag, P. Kami, J.M. Sosa, R. Banerjee, Y. Wang, H.L. Fraser, Role of ω phase in the formation of extremely refined intragranular α precipitates in metastable β-titanium alloys, Acta Mater. 103 (2016) 850–858.
- [31] T. Li, D. Kent, G. Sha, L.T. Stephenson, A.V. Ceguerra, S.P. Ringer, M.S. Dargusch, J.M. Cairney, The role of ω in the precipitation of α in near- β Ti alloys, Scripta Mater. 117 (2016) 92–95.
- [32] Y. Yang, H. Mao, H.L. Chen, M. Selleby, An assessment of the Ti–V–O system, J. Alloys Compd. 722 (2017) 365–374.
- [33] H. Lukas, S.G. Fries, B. Sundman, Computational Thermodynamics: the CALPHAD Method, Cambridge University Press, Cambridge, 2007.
- [34] Z.-K. Liu, Y. Wang, Computational Thermodynamics of Materials, Cambridge University Press, Cambridge, 2016.
- [35] P.D. Desai, Thermodynamic properties of titanium, Int. J. Thermophys. 8 (1987) 781–794.
- [36] K.K. Kelley, Specific heats at low temperatures of titanium and titanium carbide, Ind. Eng. Chem. 36 (1944) 865–866.
- [37] C.W. Kothen, H.L. Johnston, Low temperature heat capacities of inorganic solids. XVII. Heat capacity of titanium from 15 to 305 K, J. Am. Chem. Soc. 75 (1953) 3101–3102.
- [38] M.H. Aven, R.S. Craig, T.R. Waite, W.E. Wallace, Heat-capacity Measurements of Titanium and of a Hydride of Titanium for Temperatures from 4 to 15 K Including a Detailed Description of a Special Adiabatic Specific-Heat Calorimeter, National Advisory Committee for Aeronautics Rep., 1956. NACA-TN-3787.
- [39] N.M. Wolcott, The atomic heats of titanium, zirconium and hafnium, Philos. Mag. A 2 (1957) 1246–1254.
- [40] D.L. Burk, I. Estermann, S.A. Friedberg, The low temperature specific heats of titanium, zirconium and hafnium, Z. Phys. Chem. 16 (1958) 183–193.
- [41] K. Clusius, P. Franzosini, Ergebnisse der tieftemperaturforschung. XIX. Die atomund elektronenwarme des titans zwischen 13 und 273 K, Z, Phys. Chem. 16 (1958) 194–202.
- [42] G.D. Kneip Jr., J.O. Betterton Jr., J.O. Scarbrough, Low-temperature specific heats of titanium, zirconium, and hafnium, Phys. Rev. 130 (1963) 1687–1692.
- [43] R.R. Hake, J.A. Cape, Calorimetric investigation of localized magnetic moments and superconductivity in some alloys of titanium with manganese and cobalt, Phys. Rev. 135 (1964) A1151–A1160.
- [44] E.W. Collings, J.C. Ho, Magnetic susceptibility and low-temperature specific heat of high-purity titanium, Phys. Rev. B 2 (1970) 235–244.
- [45] K.L. Agarwal, J.O. Betterton, Low-temperature specific heat of Ti-Hf alloys, J. Low Temp. Phys. 17 (1974) 515–519.
- [46] M.W. Chase, NIST-JANAF Thermochemical Tables, American Institute of Physics, Washington D. C., 1998.
- [47] Y.M. Golutvin, Heat content and heat capacities in the system titanium-silicon, Russ. J. Phys. Chem. 33 (1959) 174–178.
- [48] N.N. Serebrennikov, P.V. Gel'd, Heat content and heat capacity of titanium at high temperatures, Non-Ferrous Metall. 4 (1961) 80–86.
- [49] B. Stalinski, Z. Bieganski, Rocz. Chem. 35 (1961) 273.
- [50] R. Parker, Rapid Phase Transformations in Titanium Induced by Pulse Heating, M. S. thesis, University of California, 1964.
- [51] I.I. Novikov, The effect of the degree of deformation on the thermophysical properties of metals at high temperatures, High. Temp. - High. Press. 8 (1976) 483–492.
- [52] Y.P. Zarichnyak, T.A. Lisnenko, Thermal conductivity of binary and ternary disordered solid solutions of a titanium-zirconium-hafnium system, J. Eng. Phys. 33 (1977) 1175–1179.
- [53] W.M. Cash, C.R. Brooks, The heat capacity of α-titanium from 320 to 1020 K, J. Chem. Thermodyn. 14 (1982) 351–355.
- [54] L.R. Holland, Physical properties of titanium. III. the specific heat, J. Appl. Phys. 34 (1963) 2350–2357.
- [55] I. Backhurst, Adiabatic vacuum calorimeter from 600 to 1600 $^{\circ}\text{C},$ J. Iron Steel Inst. 189 (1958) 124–134.
- [56] K.D. Maglić, D.Z. Pavičić, Thermal and electrical properties of titanium between 300 and 1900 K, Int. J. Thermophys. 22 (2001) 1833–1841.
- [57] R. Kohlhaas, M. Braun, O. Vollmer, Die atomwärme von titan, vanadin und chrom im bereich hoher temperaturen, Z. Naturforsch. 20 (1965) 1077–1079.
- [58] V.E. Peletskii, E.B. Zaretskii, in: Proc. 8th 1981 Symp. Thermophys. Prop. ASME, Vol. 2: Thermophysical Properties of Solids and Selected Fluids for Energy Technology, ASME, New York, 1982.

- [59] Y. Takahashi, High-temperature heat-capacity measurement up to 1500 K by the triple-cell DSC, Pure Appl. Chem. 69 (1997) 2263–2270.
- [60] V.O. Shestopal, Specific heat and vacancy formation in titanium at high temperatures, Sov. Phys. Solid State 7 (1966) 2798–2799.
- [61] A.V. Arutyunov, S.N. Banchila, L.P. Filippov, Properties of titanium at temperatures above 1000 K, High Temp. 9 (1971) 487–489.
- [62] E. Kaschnitz, P. Reiter, Heat capacity of titanium in the temperature range 1500 to 1900 K measured by a millisecond pulse-heating technique, J. Therm. Anal. Calorim. 64 (2001) 351–356.
- [63] A. Cezairliyan, A.P. Miiller, Heat capacity and electric resistivity of titanium in the range 1500 to 1900 K by a pulse heating method, High. Temp. - High. Press. 9 (1977) 319–324.
- [64] B. Guo, G. Teodorescu, R.A. Overfelt, P.D. Jones, Measurements of heat capacity of pure titanium and zirconium by electromagnetic levitation, Int. J. Thermophys. 29 (2008) 1997–2005.
- [65] R. Hultgren, P.D. Desai, D.T. Hawkins, M. Gleiser, K.K. Kelley, D.D. Wagman, Selected Values of Thermodynamic Properties of the Elements, ASM, Metals Park, 1973
- [66] V.P. Glushko, L.V. Gurvich, G.A. Bergman, I.V. Veitz, V.A. Medvedev, G. A. Khachkuruzov, V.S. Yungman, Thermodynamic Properties of Individual Substances, vol. IV, High-Temperature Institute of Applied. Chemistry, National Academy of Sciences of the USSR, Moscow, 1982.
- [67] J.A. Treverton, J.L. Margrave, Thermodynamic properties by levitation calorimetry III.the enthalpies of fusion and heat capacities for the liquid phases of iron, titanium, and vanadium, J. Chem. Thermodyn. 3 (1971) 473–481.
- [68] B.Y. Berezin, S.A. Kats, M.M. Kenisarin, V.Y. Chakhovskoi, Heat and melting temperature of titanium, High Temp. 12 (1974) 450–455.
- [69] P.-F. Paradis, W.-K. Rhim, Non-contact measurements of thermophysical properties of titanium at high temperature, J. Chem. Thermodyn. 32 (2000) 123–133.
- [70] G.W. Lee, S. Jeon, C. Park, D.-H. Kang, Crystal-liquid interfacial free energy and thermophysical properties of pure liquid Ti using electrostatic levitation: hypercooling limit, specific heat, total hemispherical emissivity, density, and interfacial free energy, J. Chem. Thermodyn. 63 (2013) 1–6.
- [71] K. Zhou, H.P. Wang, J. Chang, B. Wei, Experimental study of surface tension, specific heat and thermaldiffusivity of liquid and solid titanium, Chem. Phys. Lett. 639 (2015) 105–108.
- [72] T. Ishikawa, C. Koyama, Y. Nakata, Y. Watanabe, P.-F. Paradis, Spectral emissivity and constant pressure heat capacity of liquid titanium measured by an electrostatic levitator, J. Chem. Thermodyn. 131 (2019) 557–562.
- [73] Y.M. Zhang, Y.H. Zhao, H. Hou, Z.Q. Wen, M.L. Duan, Comparison of mechanical and thermodynamic properties of fcc and bcc titanium under high pressure, Mater. Res. Express 5 (2018), 026527.
- [74] Z.G. Mei, S.L. Shang, Y. Wang, Z.-K. Liu, Density-functional study of the thermodynamic properties and the pressure-temperature phase diagram of Ti, Phys. Rev. B 80 (2009) 104116.
- [75] U. Argaman, E. Eidelstein, O. Levy, G. Makov, Thermodynamic properties of titanium from ab initio calculations, Mater. Res. Express 2 (2015), 016505.
- [76] G. Cacciamani, Y.A. Chang, G. Grimvall, P. Frankes, P. Miodownik, L. Kaufman, J. M. Sanchez, M. Schalin, C. Sigli, Workshop on thermodynamic modelling of solutions and alloys, Group 3: order-disorder phase diagrams, Calphad 21 (1997) 219–246.
- [77] G. Grimvall, Thermophysical Properties of Materials, Elsevier Science, North-Holland, Amsterdam, 1986.
- [78] Q. Chen, B. Sundman, Calculation of debye temperature for crystalline structuresa case study on Ti, Zr, and Hf, Acta Mater. 49 (2001) 947–961.
- [79] K.L. Agarwal, J.O. Betterton Jr., in: Proc. 13th Int. Conf. Low Temp. Phys., vol. 4, 1974. New York.
- [80] F. Heiniger, J. Muller, Bulk superconductivity in dilute hexagonal titanium alloys, Phys. Rev. 134 (1964) A1407–A1409.
- [81] E.W. Collings, J.C. Ho, Physical properties of titanium alloys, in: R. Jaffee, N. Promisel (Eds.), The Science, Technology and Aplication of Titanium, Pergamon Press, New York, 1970, pp. 331–347.
- [82] G. Dummer, The specific heats of Zr-Rh alloys have been measured between 0.9 and 12° K, Z. Phys. 186 (1965) 249–263.
- [83] E.S. Fisher, C.J. Renken, Single-crystal elastic moduli and the hcp → bcc transformation in Ti, Zr, and Hf, Phys. Rev. 135 (1964) A482–A494.
- [84] C. Kittel, Introduction to Solid State Physics, Wiley, New York, 1996.
- [85] Q. Chen, B. Sundman, Royal Institute of Technology, Stockholm, unpublished work, 2000
- [86] W. Petry, A. Heiming, J. Trampenau, M. Alba, C. Herzig, H.R. Schober, G. Vogl, Phonon dispersion of the bcc phase of group-IV metals. I. bcc titanium, Phys. Rev. B 43 (1991) 10933–10947.
- [87] H. Ledbetter, H. Ogi, S. Kai, S. Kim, M. Hirao, Elastic constants of body-centeredcubic titanium monocrystals, J. Appl. Phys. 95 (2004) 4642–4644.
- [88] J.Y. Yan, G.B. Olson, Computational thermodynamics and kinetics of displacive transformations in titanium-based alloys, J. Alloys Compd. 673 (2016) 441–454.
- [89] C.E. Hu, Z.Y. Zeng, L. Zhang, X.R. Chen, L.C. Cai, D. Alfe, Theoretical investigation of the high pressure structure, lattice dynamics, phase transition, and thermal equation of state of titanium metal, J. Appl. Phys. 107 (2010), 093509
- [90] S. Kanemaki, M. Suzuki, Y. Yamada, U. Mizutani, Low temperature specific heat, magnetic susceptibility and electrical resistivity measurements in Ni–Ti metallic glasses, J. Phys. F Met. Phys. 18 (1988) 105–112.
- [91] K.D. Machado, Comparison between Einstein and Debye models for an amorphous Ni₄₆Ti₅₄ alloy produced by mechanical alloying investigated using

- extended X-ray absorption fine structure and cumulant expansion, J. Chem. Phys. 134 (2011), 064503.
- [92] U. Mizutani, N. Akutsu, T. Mizoguchi, Electronic properties of Cu–Ti metallic glasses, J. Phys. F Met. Phys. 13 (1983) 2127–2136.
- [93] R. Ristić, E. Babić, M. Stubičar, A. Kuršumović, J.R. Cooper, I.A. Figueroa, I. Bakonyi, Simple correlation between mechanical and thermal properties in TE-TL (TE = Ti, Zr, Hf; TL = Ni, Cu) amorphous alloys, J. Non-Cryst. Solids 357 (2011) 2949–2953.
- [94] R. Ristić, E. Babić, M. Stubičar, A. Kuršumović, Correlation between electronic structure, mechanical properties and stability of TE-TL metallic glasses, Croat. Chem. Acta 83 (2010) 33–37.
- [95] I. Bakonyi, Electronic properties and atomic structure of (Ti, Zr, Hf)–(Ni, Cu) metallic glasses, J. Non-Cryst. Solids 180 (1995) 131–150.
- [96] G. Grimvall, Thermophysical Properties of Materials, Elsevier, Netherlands, 1999.
- [97] B. Golding, B.G. Bagley, F.S.L. Hsu, Soft transverse phonons in a metallic glass, Phys. Rev. Lett. 29 (1972) 68–70.
- [98] U. Mizutani, T.B. Massalski, Low-temperature lattice specific heats of an amorphous Pd–Si alloy subjected to various heat treatments, J. Phys. F Met. Phys. 10 (1980) 1093–1100.
- [99] J.-B. Suck, H. Rudin, H.-J. Giintherodt, H. Beck, Dynamical structure factor and vibrational density of states of the metallic glass Mg₇₀Zn₃₀ measured at room temperature, J. Phys. C Solid State Phys. 14 (1981) 2305–2317.
- [100] J. Hafner, Structure and vibrational dynamics of the metallic glass Ca₇₀Mg₃₀, Phys. Rev. B 27 (1983) 678–695.
- [101] A. Cezairliyan, A.P. Miiller, Thermodynamic study of the α - β phase transformation in titanium by a pulse heating method, J. Res. Natl. Bur. Stand. 83 (1978) 127–132.
- [102] J.L. Scott, A Calorimetric Investigation of Zirconium, Titanium and Zirconium Alloys from 60 to 960 oC, 1957. USAEC Rep. ORNL-2328.
- [103] C.W. Kothen, The High Temperature Heat Contents of Molybdenum and Titanium and the Low Temperature Heat Capacities of Titanium, Ph.D. thesis, Ohio State University, Columbus, 1952.
- [104] P.V. Gel'd, Y.V. Putintsev, Tr. Ural. Politekh. Inst. 186 (1970) 199-200.
- [105] M. Harmelin, P. Lehr, C.R. Hebd, Seances Acad. Sci. Sect. C 280 (1975) 1011–1014.
- [106] E. Kaschnitz, P. Reiter, Enthalpy and temperature of the titanium alpha-beta phase transformation, Int. J. Thermophys. 23 (2002) 1339–1345.
- [107] M.M. Martynyuk, V.I. Tsapkov, Electric resistance, enthalpy and phase transformations of titanium, zirconium and hafnium during pulse heating, Izv. Akad. Nauk. SSSR, Met. 1 (1974) 181–188.
- [108] D.W. Bonnell, Property Measurements at High Temperatures-Levitation Calorimetry Studies of Liquid Metals, Ph.D. Thesis, Rice University, Houston, Tex, 1972.
- [109] Y. Wang, S. Curtarolo, C. Jiang, R. Arroyave, T. Wang, G. Ceder, Z.K. Liu, Ab initio lattice stability in comparison with CALPHAD lattice stability, Calphad 28 (2004) 79–90.
- [110] J. Vřešť ál, J. Štrof, J. Pavlů, Extension of SGTE data for pure elements to zero Kelvin temperature-A case study, Calphad 37 (2012) 37–48.
- [111] The OQMD database. http://oqmd.org.
- [112] D.A. Mirzaev, V.M. Schastlivtsev, O.A. Elkina, V.G. Ul'yanov, Rapid cooling effect on polymorphous transformation in titanium-molybdenum alloys, Fiz. Met. Metalloved. 81 (1996) 87–96.
- [113] K. Thurnay, Thermal Properties of Transition Metals, Forschungszentrum Karlsruhe GmbH Technik und Umwelt, Inst. fuer Neutronenphysik und Reaktortechnik, 1998.
- [114] J.F. Smith, The V (vanadium) system, J. Phase Equil. 2 (1981) 40-41.
- [115] P.D. Desai, Thermodynamic properties of vanadium, Int. J. Thermophys. 7 (1986) 213–228.
- [116] J.W. Arblaster, Thermodynamic properties of vanadium, J. Phase Equilibria Diffus. 38 (2017) 51–64.
- [117] K.D. Maglić, Recommended specific heat capacity functions of group VA elements, Int. J. Thermophys. 24 (2003) 489–500.
- [118] C.T. Anderson, The heat capacities of vanadium, vanadium trioxide, vanadium tetroxide and vanadium pentoxide at low temperatures, J. Am. Chem. Soc. 58 (1936) 564–566.
- [119] K. Clusius, P. Franzosini, U. Piesbergen, Ergebnisse der tieftemperaturforschung. XXXII. Die atom-und elektronenwärme des vanadins und niobs zwischen 10 und 273° K, Z. Naturforsch. 15 (1960) 728–734.
- [120] Z. Bieganski, B. Stalinski, Heat capacities and thermodynamic functions of vanadium and vanadium hydride within the range 24 to 340°K: the hydrogen contribution to the heat capacity of transition metal hydrides, Bull. Acad. Polon. Sci. Ser. Sci. Chim. 9 (1961) 367–372.
- [121] M. Ishikawa, L.E. Toth, Electronic specific heats and superconductivity in the group-V transition metals, Phys. Rev. B 3 (1971) 1856–1861.
- [122] N.A. Chernoplekov, G.K. Panova, B.N. Samoilov, A.A. Shikov, Change of the vanadium phonon spectrum following introduction of tantalum admixtures, Sov. Phys. JETP 36 (1973) 731–735.
- [123] W.S. Corak, B.B. Goodman, C.B. Satterthwaite, Exponential temperature dependence of the electronic specific heat of superconducting vanadium, Phys. Rev. 96 (1954) 1442–1444.
- [124] R.D. Worley, M.W. Zemansky, H.A. Boorse, Heat capacities of vanadium and tantalum in the normal and superconducting phases, Phys. Rev. 99 (1955) 447–458.
- [125] W.S. Corak, B.B. Goodman, C.B. Satterthwaite, Atomic heats of normal and superconducting vanadium, Phys. Rev. 102 (1956) 656–661.

- [126] C.H. Cheng, K.P. Gupta, E.C. Van Reuth, P.A. Beck, Low-temperature specific heat of body-centered cubic Ti–V alloys, Phys. Rev. 126 (1962) 2030–2033.
- [127] P.H. Keesom, R. Radebaugh, Mixed-state specific heat of vanadium at very low temperatures, Phys. Rev. Lett. 13 (1964) 685–686.
- [128] Y.L. Shen, I. Low Temperature Heat Capacities of Vanadium, Niobium and Tantalum, II. Low Temperature Heat Capacity of Ferromagnetic Chromic Tribromid, Ph.D. thesis, University of California, Berkeley, 1965.
- [129] R. Radebaugh, P.H. Keesom, Low-temperature thermodynamic properties of vanadium. I. Superconducting and normal states, Phys. Rev. 149 (1966) 209–216.
- [130] N.A. Chernoplekov, G.K. Panova, B.N. Samoilov, A.A. Shikov, Alteration of the superconducting properties of vanadium by the introduction of tantalum impurity atoms, Sov. Phys. JETP 37 (1973) 102–106.
- [131] K. Kumagai, T. Ohtsuka, The superconductivity of alloys of a transition metal with non-transition elements, J. Phys. Soc. Jpn. 37 (1974) 384–392.
- [132] G.J. Sellers, M. Paalanen, A.C. Anderson, Anomalous heat capacity of superconducting vanadium, Phys. Rev. B 10 (1974) 1912–1915.
- [133] G.H. Comsa, D. Heitkamp, H.S. R\u00e4de, Specific heat of ultrafine vanadium particles in the temperature range 1.3-10 K, Solid State Commun. 20 (1976) 877–880.
- [134] H.A. Leupold, G.J. Iafrate, F. Rothwarf, J.T. Breslin, D. Edmiston, T.R. AuCoin, Low-temperature specific heat anomalies in the group V transition metals, J. Low Temp. Phys. 28 (1977) 241–261.
- [135] D. Ohlendorf, E. Wicke, Heat capacities between 1.5 and 16 K and superconductivity of V/H and Nb/H alloys, J. Phys. Chem. Solid. 40 (1979) 721–728.
- [136] Y. Takahashi, J.I. Nakamura, J.F. Smith, Laser-flash calorimetry III. Heat capacity of vanadium from 80 to 1000 K, J. Chem. Thermodyn. 14 (1982) 977–982.
- [137] F.M. Jaeger, W.A. Veenstra, The exact measurement of the specific heats of solid substances at high temperatures. VI. The specific heats of vanadium, niobium, tantalum and molybdenum, Rec. Trav. Chim. 53 (1934) 677–687.
- [138] G.C. Beakley Jr., Ph.D. thesis, Oklahoma State University, Stillwater, 1956.
- [139] R.A. Knezek, M.S. thesis, Oklahoma State University, Stillwater, 1959.
- [140] I.B. Fieldhouse, J.I. Lang, Measurement of Thermal Properties, Armour Research Foundation Chicago IL, 1961.
- [141] Y.M. Golutvin, T.M. Kozlovskaya, Enthalpy and heat capacity in the vanadiumsilicon system, Russ. J. Phys. Chem. 36 (1962) 183–185.
- [142] M. Braun, R. Kohlhaas, O. Vollmer, Hightemperature calorimetry of metals, Z. Angew. Phys. 25 (1968) 365–372.
- [143] L.P. Filippov, R.P. Yurchak, High-temperature investigations of the thermal properties of solids, J. Eng. Phys. Thermophys. 21 (1971) 1209–1220.
- [144] V.E. Peletskii, V.P. Druzhinin, Y.G. Sobol, Thermophysical properties of vanadium at high temperatures, High. Temp. - High. Press. 3 (1971) 153–159.
- [145] J.L. Margrave, Studies in the Physical Chemistry of Selected High Temperature Systems, Rice Univ. Rep., 1972. ORO-2907-92.
- [146] A.V. Arutyunov, I.N. Makarenko, L.P. Filippov, Thermal properties of vanadium at high temperature, Teplofiz, Svoistva Veshchestv Mater 5 (1972) 105–108.
- [147] V. Chekhovskoi, R.G. Kalinkina, Specific heat of V in the temperature range 300-900 K, Teplofiz. Vysok. Temp. 11 (1973) 885–886.
- [148] B.E. Neimark, P.E. Belyakova, B.R. Brodskii, L.K. Voronin, S.F. Korytina, A. N. Merkul'ev, Physical properties of vanadium, Heat Tran. Sov. Res. 5 (1973) 141–145
- [149] A. Cezairliyan, F. Righini, J.L. McClure, Simultaneous measurements of heat capacity, electrical resistivity, and hemispherical total emittance by a pulse heating technique: vanadium, 1500 to 2100 K, J. Res. Natl. Bur. Stand. 78A (1974) 143–147.
- [150] B.Y. Berezin, V.Y. Chekhovskoi, Enthalpy and heat capacity of niobium and vanadium in the temperature range from 298.15 K to the melting point, High Temp. 15 (1977) 651–657.
- [151] A.A. Kulish, L.P. Filippov, Determination of the physical properties of group V metals at high temperatures by means of a study of deformation vibrations of plates, High Temp. 16 (1978) 512–519.
- [152] W. Bendick, W. Pepperhoff, The heat capacity of Ti, V and Cr, J. Phys. F Met. Phys. 12 (1982) 1085–1090.
- [153] A. Stanimirović, G. Vuković, K. Maglić, Thermophysical and thermal optical properties of vanadium by millisecond calorimetry between 300 and 1900 K, Int. J. Thermophys. 20 (1999) 325–332.
- [154] V.Y. Chekhovskoii, V.D. Tarasov, N.V. Grigor'eva, Contribution of equilibrium vacancies to vanadium caloric properties, High Temp. 49 (2011) 826–831.
- [155] B.Y. Berezin, V.Y. Chekhovskoi, A.E. Sheindlin, Enthalpy and specific heat of molten vanadium, High Temp. Sci. 4 (1972) 478–486.
- [156] R. Lin, M.G. Frohberg, Enthalpy measurements on solid and liquid vanadium by levitation calorimetry, Z. Metallkd. 82 (1991) 48–52.
- [157] D.D. Martin Southern, M.S. thesis, Methodist University, Dallas, Tex, 1963.
- [158] E.C. van Reuth, Ph.D. thesis, University of Illinois, Urbana, 1964.
- [159] F. Heiniger, E. Bucher, J. Muller, Low temperature specific heat of transition metals and alloys, Phys. kondens. Materie 5 (1966) 243–284.
- [160] A. Junod, F. Heiniger, J. Mueller, P. Spitzli, Superconductivity and specific heat of alloys based on Ti₃Sb, Helv. Phys. Acta 43 (1970) 59–66.
- [161] J.M. Corsan, A.J. Cook, Specific heat and superconductivity of binary alloys containing V, Nb, and Ta, Phys. Status Solidi 40 (1970) 657–665.
- [162] V.M. Pan, V.G. Prokhorov, A.D. Shevchenko, V.P. Dovgopol, Investigation of physical properties of vanadium in the temperature range of 4.2 to 300 K, Fiz. Nizk. Temp. 3 (1977) 1266–1271.
- [163] O. Vergara, D. Heitkamp, H.V. Löhneysen, Specific heat of small vanadium particles in the normal and superconducting state, J. Phys. Chem. Solid. 45 (1984) 251–258.

[164] A.F. Guillermet, G. Grimvall, Homology of interatomic forces and Debye temperatures in transition metals, Phys. Rev. B 40 (1989) 1521–1527.

- [165] G.A. Iglesias-Silva, K.R. Hall, Simple expressions for the heat capacities of elemental solids, Chem. Eng. Commun. 158 (1997) 193–199.
- [166] Z.M. Tomilo, Debye temperature in the high-temperature limit and anharmonic component of the heat capacity of vanadium, J. Eng. Phys. Thermophys. 51 (1986) 962–964.
- [167] X.B. Li, Y.Q. Xie, Y.Z. Nie, H.J. Peng, Low temperature thermodynamic study of the stable and metastable phases of vanadium, Chin. Sci. Bull. 52 (2007) 3041–3046.
- [168] G.R. Gathers, J.W. Shaner, R.S. Hixson, D.A. Young, Very high temperature thermophysical properties of solid and liquid vanadium and iridium, High. Temp. - High. Press. 11 (1979) 653–668.
- [169] U. Seydel, H. Bauhof, W. Fucke, H. Wadle, Thermophysical data for various transition metals at high temperatures obtained by a submicrosecond-pulseheating method, High. Temp. - High. Press. 11 (1979) 635–642.
- [170] K. Schaefers, M. Rösner-Kuhn, M.G. Frohberg, Enthalpy measurements of undercooled melts by levitation calorimetry: the pure metals nickel, iron, vanadium and niobium, Mater. Sci. Eng., A 197 (1995) 83–90.
- [171] G. Pottlacher, T. Hüpf, B. Wilthan, C. Cagran, Thermophysical data of liquid vanadium, Thermochim. Acta 461 (2007) 88–95.
- [172] E. Rudy, S. Windisch, The phase diagrams hafnium-vanadium and hafnium-chromium, J. Less Common. Met. 15 (1968) 13–27.
- [173] J.-P. Hiernaut, F. Sakuma, C. Ronchi, Determination of the melting point and the emissivity of refractory metals with a six-wavelength pyrometer, High. Temp. -High. Press. 21 (1989) 139–148.
- [174] J.L. McClure, A. Cezairliyan, Radiance temperatures (in the wavelength range 525 to 906 nm) of vanadium at its melting point by a pulse-heating technique, Int. J. Thermophys. 18 (1997) 291–302.
- [175] N. Saunders, System Ti-V, in: I. Ansara, A.T. Dinsdale, M.H. Rand (Eds.), COST 507-Thermochemical Database for Light Metal Alloys, Office for Official Publications of the European Communities, Luxembourg, 1998.
- [176] J.Y. Lee, J.H. Kim, S.I. Park, H.M. Lee, Phase equilibrium of the Ti–Cr–V ternary system in the non-burning β-Ti alloy region, J. Alloys Compd. 291 (1999) 229–238.
- [177] G. Ghosh, Thermodynamic and kinetic modeling of the Cr–Ti–V system, J. Phase Equil. 23 (2002) 310–328.
- [178] G. Lindwall, P.S. Wang, U.R. Kattner, C.E. Campbell, The effect of oxygen on phase equilibria in the Ti-V system: impacts on the AM processing of Ti alloys, JOM 70 (2018) 1692–1705.
- [179] J.L. Murray, The Ti-V (titanium-vanadium) system, Bull. Alloy Phase Diagrams 2 (1981) 48-55.
- [180] J.L. Murray, Ti–V (titanium-vanadium), in: T.B. Massalski, H. Okamoto, P. R. Subramanian, L. Kacprzak (Eds.), Binary Alloy Phase Diagrams, ASM International, 1987.
- [181] O. Nakano, H. Sasano, T. Suzuki, H. Kimura, in: H. Kimura, O. Izumi (Eds.), Titanium'80, Proc. 4th Int. Conf. On Titanium, Kyoto, Japan vol. 2, 1980, pp. 2889–2895
- pp. 2669–2693.

 [182] W. Fuming, H.M. Flower, Phase separation reactions in Ti–50V alloys, Mater. Sci. Technol. 5 (1989) 1172–1177
- [183] H.K. Adenstedt, J.R. Pequignot, J.M. Raymer, The Ti–V system, Trans. A. S. M. 44 (1952) 990–1003.
- [184] E. Rudy, Ternary Phase Equilibria in Transition Metal-Boron-Carbon-Silicon Systems. Part 5. Compendium of Phase Diagram Data (Compendium of Phase Diagram Data, U.S. Air Force Rep. AFML-TR-65-2, Pt. IV), Aerojet-general corp sacramento ca materials research lab, 1969.
- [185] A.D. McQuillan, The effect of the elements of the first long period on the α - β transformation in titianium, J. Inst. Met. 80 (-52) (1951) 363–368.
- [186] F. Ermanis, P.A. Farrar, H. Margolin, A reinvestigation of the systems Ti–Cr and Ti–V, Trans. AIME 221 (1961) 904–908.
- [187] S.G. Fedotov, K.M. Konstantinov, E.P. Sinodova, Disintegration of titanium-vanadium martensite on continuous heating, Phys. Met. Metallogr. 25 (1968) 104–110
- [188] G.N. Ronami, Determination of phase equilibria of superconducting alloys using the mass spectrometer, Krist. Tech. 7 (1972) 615–638.
- [189] V.V. Molokanov, D.B. Chernov, P.B. Budberg, Solubility of vanadium in α titanium, Met. Sci. Heat Treat. 19 (1977) 704–705.
- [190] E.J. Rolinski, M. Hoch, C.J. Oblinger, Determination of thermodynamic interaction parameters in solid V-Ti alloys using the mass spectrometer, Metall. Trans. 2 (1971) 2613–2618.
- [191] K.C. Mills, K. Kinoshita, Activities of liquid titanium+ vanadium alloys, J. Chem. Thermodyn. 5 (1973) 129–133.
- [192] T. Uesugi, S. Miyamae, K. Higashi, Enthalpies of solution in Ti–X (X = Mo, Nb, V and W) alloys from first-principles calculations, Mater. Trans. 54 (2013) 484–492.
- [193] R. Chinnappan, B.K. Panigrahi, A. van de Walle, First-principles study of phase equilibrium in Ti–V, Ti–Nb, and Ti–Ta alloys, Calphad 54 (2016) 125–133.
- [194] K.K. McCabe, S.L. Sass, The initial stages of the omega phase transformation in Ti–V alloys, Philos. Mag. A 23 (1971) 957–970.
- [195] C. Leibovitch, A. Rabinkin, M. Talianker, Phase transformations in metastable Ti–V alloys induced by high pressure treatment, Metall. Mater. Trans. 12 (1981) 1513–1519.
- [196] L.C. Ming, M.H. Manghnani, K.W. Katahara, Phase transformations in the Ti–V system under high pressure up to 25 GPa, Acta Metall. 29 (1981) 479–485.
- [197] H. Matsumoto, S. Watanabe, N. Masahashi, S. Hanada, Composition dependence of Young's modulus in Ti–V, Ti–Nb, and Ti–V–Sn alloys, Metall. Mater. Trans. 37 (2006) 3239–3249.

- [198] A.V. Dobromyslov, V.A. Elkin, The orthorhombic α"-phase in binary titanium-base alloys with d-metals of V–VIII groups, Mater. Sci. Eng., A 438 (2006) 324–326.
- [199] G. Aurelio, A.F. Guillermet, G.J. Cuello, J. Campo, Metastable phases in the Ti–V system: Part I. Neutron diffraction study and assessment of structural properties, Metall. Mater. Trans. 33 (2002) 1307–1317.
- [200] C. Ghosh, J. Basu, D. Ramachandran, E. Mohandas, Phase separation and ω transformation in binary V–Ti and ternary V–Ti–Cr alloys, Acta Mater. 121 (2016) 310–324
- [201] D. Choudhuri, Y. Zheng, T. Alam, R. Shi, M. Hendrichson, S. Banerjee, Y. Wang, S. G. Srinivasan, H. Fraser, R. Banerjee, Coupled experimental and computational investigation of omega phase evolution in a high misfit titanium-vanadium alloy, Acta Mater. 130 (2017) 215–228.
- [202] H. Kaneko, Y.C. Huang, Some considerations on the continuous cooling diagrams and M_s points of titanium-base alloys, J. Jpn. Inst. Metals 27 (1963) 403–406.
- [203] Y.C. Huang, S. Suzuki, H. Kaneko, T. Sato, Thermodynamics of the M_s points in titanium alloys, in: R. Jaffee, N. Promisel (Eds.), The Science, Technology and Application of Titanium, Pergamon Press, Oxford, 1970, pp. 691–693.
- [204] A.V. Dobromyslov, V.A. Elkin, Martensitic transformation and metastable β-phase in binary titanium alloys with d-metals of 4-6 periods, Scr. Meter. 44 (2001) 905–910.
- [205] P. Duwez, Effect of rate of cooling on the alpha-beta transformation in titanium and titanium-molybdenum alloys, Trans. AIME 191 (1951) 765–771.
- [206] T. Sato, S. Hukai, Y.C. Huang, The M_s points of binary titanium alloys, Austral. Inst. Met. 5 (1960) 149–153.
- [207] K. Bungardt, K. Ruedinger, Phase transformations in titanium-molybdenum alloys, Z. Metallkd. 52 (1961) 120–135.
- [208] H. Kaneko, Y.C. Huang, Allotropic transformation characteristics of titanium alloys during continuous cooling, J. Jpn. Inst. Metals 27 (1963) 387–393.
- [209] R. Davis, H.M. Flower, D.R.F. West, Martensitic transformations in Ti-Mo alloys, J. Mater. Sci. 14 (1979) 712–722.
- [210] P. Pietrokowsky, P. Duwez, Partial titanium-vanadium phase diagram, JOM 4 (1952) 627–630.
- [211] N.E. Paton, J.C. Williams, The influence of oxygen content on the athermal β - ω transformation, Scripta Metall. 7 (1973) 647–649.
- [212] D.A. Mirzaev, V.G. Ul'yanov, M.M. Shtejnberg, V.A. Protopopov, Structural and kinetic steps of $\beta \to \alpha$ transformation in titanium, Fiz. Met. Metalloved. 51 (1981) 115–122.
- [213] M. Ikeda, S.Y. Komatsu, T. Sugimoto, K. Kamei, Resistometric estimation of temperature range of athermal ω phase formation in quenched Ti–V alloys, J. Jpn. Inst. Metals 54 (1990) 743–751.
- [214] N.A. Zarkevich, D.D. Johnson, Titanium α-ω phase transformation pathway and a predicted metastable structure, Phys. Rev. B 93 (2016), 020104.
- [215] S.Z. Zhang, H. Cui, M.M. Li, H. Yu, L. Vitos, R. Yang, Q.M. Hu, First-principles study of phase stability and elastic properties of binary Ti–xTM (TM = V, Cr, Nb, Mo) and ternary Ti–15TM–yAl alloys, Mater. Des. 110 (2016) 80–89.
- [216] W. Mei, J. Sun, Y. Wen, A first-principles study of displacive β to ω transition in Ti–V alloys, Prog. Nat. Sci. : Met. Mater. Int. 27 (2017) 703–708.

- [217] B. Hu, Y. Jiang, J. Wang, B. Yao, F. Min, Y. Du, Thermodynamic calculation of the T₀ curve and metastable phase diagrams of the Ti–M (M = Mo, V, Nb, Cr, Al) binary systems, Calphad 62 (2018) 75–82.
- [218] P. Hohenberg, W. Kohn, Inhomogeneous electron gas, Phys. Rev. 136 (1964) B864–B871.
- [219] W. Kohn, L.J. Sham, Self-consistent equations including exchange and correlation effects, Phys. Rev. 140 (1965) A1133–A1138.
- [220] P. Giannozzi, S. Baroni, N. Bonini, M. Calandra, R. Car, C. Cavazzoni, D. Ceresoli, G.L. Chiarotti, M. Cococcioni, I. Dabo, A. Dal Corso, S. Fabris, G. Fratesi, S. de Gironcoli, R. Gebauer, U. Gerstmann, C. Gougoussis, A. Kokalj, M. Lazzeri, L. Martin-Samos, N. Marzari, F. Mauri, R. Mazzarello, S. Paolini, A. Pasquarello, L. Paulatto, C. Sbraccia, S. Scandolo, G. Sclauzero, A.P. Seitsonen, A. Smogunov, P. Umari, R.M. Wentzcovitch, Quantum espresso: a modular and open-source software project for quantum simulations of materials, J. Phys. Condens. Matter 21 (2009) 395502.
- [221] D. Vanderbilt, Soft self-consistent pseudopotentials in a generalized eigenvalue formalism, Phys. Rev. B 41 (1990) 7892–7895.
- [222] J.P. Perdew, K. Burke, M. Ernzerhof, Generalized gradient approximation made simple, Phys. Rev. Lett. 77 (1996) 3865–3868.
- [223] H.J. Monkhorst, J.D. Pack, Special points for Brillouin-zone integrations, Phys. Rev. B 13 (1976) 5188–5192.
- [224] M. Methfessel, A.T. Paxton, High-precision sampling for Brillouin-zone integration in metals, Phys. Rev. B 40 (1989) 3616–3621.
- [225] S.R. Billeter, A. Curioni, W. Andreoni, Efficient linear scaling geometry optimization and transition-state search for direct wavefunction optimization schemes in density functional theory using a plane-wave basis, Comput. Mater. Sci. 27 (2003) 437–445.
- [226] R. Golesorkhtabar, P. Pavone, J. Spitaler, P. Puschnig, C. Draxl, ElaStic: a tool for calculating second-order elastic constants from first principles, Comput. Phys. Commun. 184 (2013) 1861–1873.
- [227] O.L. Anderson, A simplified method for calculating the debye temperature from elastic constants, J. Phys. Chem. Solid. 24 (1963) 909–917.
- [228] J.-O. Andersson, A.F. Guillermet, P. Gustafson, M. Hillert, B. Jansson, B. Jönsson, B. Sundman, J. Ågren, A new method of describing lattice stabilities, Calphad 11 (1987) 93–98.
- [229] B. Sundman, U.R. Kattner, M. Hillert, M. Selleby, J. Ågren, S. Bigdeli, Q. Chen, A. Dinsdale, B. Hallstedt, A. Khvan, H.H. Mao, R. Otis, A method for handling the extrapolation of solid crystalline phases to temperatures far above their melting point, Calphad 68 (2020) 101737.
- [230] J. Agren, Thermodynamics of supercooled liquids and their glass transition, Phys. Chem. Liq. 18 (1988) 123–139.
- [231] O. Redlich, A.T. Kister, Algebraic representation of thermodynamic properties and the classification of solutions, Ind. Eng. Chem. 40 (1948) 345–348.
- [232] B. Sundman, B. Jansson, J.-O. Andersson, The thermo-calc databank system, Calphad 9 (1985) 153–190.
- [233] F. Mouhat, F.-X. Coudert, Necessary and sufficient elastic stability conditions in various crystal systems, Phys. Rev. B 90 (2014) 224104.